Mercury accumulation in permafrost peatlands in relation to peat accumulation and permafrost history

Charlotte Haugk[1,3], Anica Brach[1], Gustaf Hugelius[2,3], Peter Kuhry[2,3], A. Britta K. Sannel[2,3], Brittany Tarbier[2], Sofi Jonsson[1,3]

[1] Department of Environmental Science, Stockholm University

[2] Department of Physical Geography, Stockholm University, Stockholm, Sweden

[3] Bolin Centre for Climate Research, Stockholm University, Stockholm, Sweden

SUMMARY

Northern peatlands act as a globally important sink for atmospheric mercury (Hg). However, the environmental drivers that control long-term Hg accumulation rates (Hg-AR) in permafrost peatland systems remain understudied. With the aim to shed light on the influence of peat accumulation conditions and permafrost formation history on Hg accumulation, we have investigated Hg profiles in nine peat cores, which have previously been characterised using plant macrofossil analyses to reconstruct peat accumulation history. Across all cores, originating from sites in west-central Canada (n = 4) and northern Scandinavia (n = 5), highest Hg concentrations were found close to the peat surface with a maximum around 220 (μg Hg kg^{-1}). Vertical profiles of Hg across successions of peat types in the cores revealed peaks of Hg concentrations in layers typical of drier surface conditions and slower peat accumulation. Calculated long-term Hg-ARs ranged from 0.3 to 2.6 μg Hg m^{-2} yr^{-1} between sites and were closely related to long-term carbon accumulation rates (C-AR). Our study shows that the net C-AR controls Hg-AR in Arctic permafrost peatlands. We further demonstrate that epigenetic permafrost accumulated twice as much Hg for the same amount of C, likely due to Hg enrichment during long-term peat decomposition in epigenetic as opposed to syngenetic permafrost peatlands.

KEY WORDS: mercury-carbon couplings, plant macrofossils, peat decomposition, syngenetic permafrost, epigenetic permafrost, Scandinavia, Canada

INTRODUCTION

Mercury is a global pollutant that is transported to the Arctic through atmospheric pathways. A fraction of this Hg is bioaccumulated in aquatic food webs, resulting in levels of concern for both human and wildlife health (*AMAP Assessment 2021*). Most of the Hg entering the Arctic, however, gets sequestered in the terrestrial compartment, including permafrost peatlands. The sequestration of Hg in northern permafrost soils is primarily driven by atmospheric uptake of elemental mercury (Hg^0) via plant foliage and subsequent incorporated into soils through litterfall where it accumulates over time due to limited Hg mobility (Obrist *et al*., 2017; Sun & Branfireun, 2023). In addition to Hg's strong affinity to organic matter, decelerated peat decomposition rates and suppressed biogeochemical transformations (typical of cold permafrost environments) has helped to facilitate the capturing of Hg in permafrost peatlands (Klaminder *et al*., 2008; Rydberg *et al*., 2010a; Talbot *et al*., 2017). Over time, this has resulted in a large stock of Hg currently stored in northern permafrost peatlands. A recent study estimates that northern permafrost soils store 600 Gg (range: 380 – 750) of Hg in the upper 3 m of the soils (Lim *et al*., 2020). Current estimates of Hg stocks in permafrost soils are, however, associated with large uncertainties, in particularly for the uppermost organic rich soil (stocks estimated for the 0 – 30 cm; Olson *et al*., 2018: 26 (21 – 42) Gg Hg, Schuster *et al*., 2018: 347 ± 196 Gg Hg and Lim *et al*., 2020: 72 (39 – 91) Gg Hg).

As in other environmental compartments, the cycling of Hg in peat is tightly coupled to the cycling of carbon (C). Jiskra *et al*. (2018), for example, demonstrated that seasonal variations of atmospheric Hg_0 in the northern hemisphere follow fluctuations in CO_2, a phenomenon that was linked to the sequestration of both Hg and C from air through plant biomass production. In peatlands, the net accumulation of C is driven by several factors, including mean annual air temperature (Hugelius *et al*., 2020), length of the growing season (Charman *et al*., 2013), as well as the composition of the vegetation cover (Mathijssen *et al*., 2019). These factors may also control the concentration of Hg in plant litter. Higher Hg concentrations are, for example, typically reported in non-vascular plants, including *Sphagnum* (peat moss), compared to vascular plants such as e.g. *Betula nana* (dwarf birch) (Olson *et al*., 2019). In addition to the fact that non-vascular plants obtain nutrients and water directly from the atmosphere, their high surface area and longer lifespan have been suggested to contribute to their greater capacity for Hg accumulation. The extensive capture of C and Hg over time in permafrost peatlands has been facilitated, as mentioned above, by limited peat decomposition in the Arctic system. In addition to the presence of permafrost, permafrost formation history has been shown to influence net sequestration of C (Vitt *et al*., 2000; Treat *et al*., 2016). Syngenetic permafrost systems, where peat and permafrost accumulated simultaneously, typically contain less decomposed peat, likely more susceptible to decomposition upon thaw in comparison to epigenetic permafrost systems, where the permafrost developed after the peat was formed (Manies *et al*., 2021). Epigenetic permafrost systems are associated with lower net C accumulation rates and C/N ratios (Vardy *et al*., 2000; O'Donnell *et al*., 2012; Treat *et al*., 2016). To date, the influence of permafrost aggregation history on Hg accumulation remains unexplored, despite the close coupling between Hg and C cycling in peatlands and the potential for Hg remobilization during peat decomposition (Klaminder *et al*., 2008; Fahnestock *et al*., 2019). To further advance our understanding of Hg accumulation in permafrost peatland systems, where Hg concentrations are known to track those of C (Schuster *et al*., 2018; Olson *et al*., 2018; Lim *et al*., 2020; Tarbier *et al*., 2021), the role of past peat and permafrost accumulation histories should be examined. Here, we have investigated the concentration and accumulation of Hg and C together with previously characterised plant macrofossil data, and data on C/N ratios as indicator of peat decomposition degree, in two syngenetic and seven epigenetic permafrost peat cores that were collected from peatlands in west-central Canada and northern Scandinavia. We hypothesize that the net carbon accumulation rate (C-ARs) as well as the permafrost formation history of the peatland affects Hg concentrations and net mercury accumulation rate (Hg-AR).

METHODS

Site and core description

All peat cores were collected within the sub-Arctic climatic zone, but in areas with different permafrost distribution and formation history (Figure 1) (Kuhry (1998, 2008), Sannel & Kuhry (2008, 2009), Markkula & Kuhry (2020), Sannel *et al*., (2018) and Kjellman *et al.* (2018)). A summary of the Holocene development, peat and C-ARs are outlined below (for further details, see references listed in Table 1).

Peatland formation at **Ennadai Lake** and **Selwyn Lake** began around 5900 and 6600 cal. yr BP, respectively (Sannel & Kuhry, 2008). At Ennadai Lake permafrost conditions likely prevailed already at the time of peatland initiation, but were followed by ground collapse and permafrost-free fen conditions between 5700 – 4700 cal. yr BP. From around 4700 cal. yr BP and onwards the Ennadai Lake site has been a peat plateau with stable permafrost conditions. At Selwyn Lake peatland initiation probably occurred under permafrost-free conditions. Apart from a short period of permafrost collapse between 4600 – 4400 cal. yr BP, permafrost aggradation and peat plateau development prevailed from around 5600 cal. yr BP until present. At both sites the peat plateau stage is characterised by alternating layers of *Sphagnum fuscum* and rootlet peat, a layer containing plant remains such as roots, twigs and leaves of xerophytic plants. Rootlet peat is associated with dry phases (e.g. dry bog) and can be indicative for permafrost conditions when rootlet layers repeatedly alternate with *Sphagnum fuscum* layers (Oksanen *et al*., 2001, 2003). In the lower part of the Ennadai Lake core, between 180 – 135 cm depth, the peat consists of wet growing *Sphagnum* mosses and other fen indicators. Detailed plant macrofossil analysis suggests that there were no permafrost conditions at the time these layers were formed and that they have been exposed to anaerobic decay. For both cores, peat accumulation rates (peat AR) were calculated to around 0.3 mm yr^{-1} (Sannel & Kuhry, 2009), which is in agreement with average peat ARs for sub-Arctic Canadian peatlands suggested by Gorham (1991). The net C-AR was around 13 g C m^{-2} yr^{-1}. Sannel & Kuhry (2009) calculated that the rootlet peat layers have 4-5 times lower peat ARs, and 3 – 4 times lower net C-ARs, than the *Sphagnum* peat layers. The lowest peat and net C-ARs were reported for the upper rootlet layer (e.g. for Ennadai Lake: 0.04 mm yr^{-1} and 3.7 g C m^{-2} yr^{-1}) likely due to erosion or wind abrasion following frost heave. At Selwyn Lake the rootlet peat stages accounted for about half (56%) of the time since the peatland was initiated, even though *Sphagnum* made up the majority of the gross stratigraphy in the peat profile.

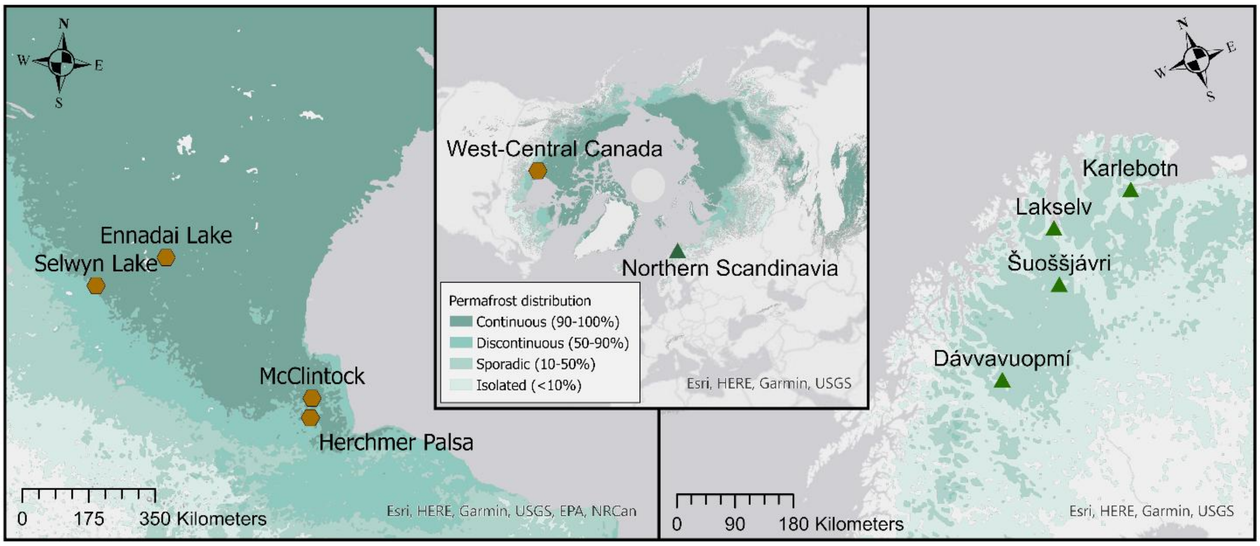

Figure 1. Location of study sites in west-central Canada (A and B) and northern Scandinavia (B and C). Shaded areas shows the permafrost distribution (adapted from Obu *et al.*, (2018)) with isolated (< 10%), sporadic (10 – 50%), discontinuous (50 – 90%) and continuous (90 – 100%) permafrost distribution. Maps were generated using ArcGIS Pro 3.3.

The **Herchmer Palsa** and **McClintock peat plateaus** developed through paludification as wet rich fens under permafrost-free conditions from previously forested uplands at c. 6900 and 6700 cal. yr BP (Kuhry, 2008; Markkula & Kuhry, 2020). Permafrost aggradation at Herchmer Palsa was dated to AD 1958 ± 3 yr (30 years before the core was extracted), while at McClintock the permafrost history has been more complex with several phases of aggradation and collapse. Colder climatic conditions resulted in permafrost aggradation at > 2250 cal. yr BP, and dry surface conditions altered the vegetation as a result of frost heave. After the permafrost collapsed, an intermediate open poor fen became established for the next 1800 years. A second permafrost stage developed similar to the first one around 450 cal. yr BP. This was followed by yet another brief period of collapse after which the most recent peat plateau stage developed.

At two sites in northern Sweden, **Alvi** and **Dávva**, peatland development began around 10 000 cal. yr BP (in Alvi) and 6000 cal. yr BP (in Dávva) (Sannel *et al.*, 2018). During much of the Holocene, both sites have permafrost-free fen characteristics, with stable and low C/N ratios. The subsequent transition from fen to dry bog conditions following permafrost inception took place c. 600 – 100 cal. yr BP. There appear to be no clear indications of permafrost aggradation prior to the Little Ice Age during the Holocene. C-ARs varied over time but were generally higher in the early to mid-Holocene, followed by lower ARs in the late Holocene. Long-term net C-ARs were calculated to around 10.2 and 13.5 g C m^{-2} yr^{-1} for Alvi and Dávva with very low rates at Alvi (< 2 g C m^{-2} yr^{-1}) from around 2700 – 2100 cal. yr BP until 400 – 100 cal. yr BP, probably due to hiatus in the peat sequence.

In **Šuoššjávri**, located in an upland area of Finnmark (northern Norway) peatland development started around 9800 cal. yr BP (Kjellman *et al.*, 2018). Since coastal areas lay below sea level for several thousand years after the deglaciation, peatland initiation in **Lakselv** and **Karlebotn** did not occur until the mid-Holocene (c. 6150 and 5150 cal. yr BP, respectively). At all three Norwegian sites the peatlands started to form as fens and remained permafrost-free throughout the majority of the Holocene. Considerably cooler climate during the Little Ice Age likely led to permafrost initiation and peat plateau development during the last millennium (c. 950 – 100 cal. yr BP). In the Karlebotn core, a possible earlier period of permafrost (ca 2200 cal. yr BP (Kjellman *et al.*, 2018); or ca 3000 cal. yr BP (Hichens-Bergström & Sannel, 2023) was suggested by the presence of *Sphagnum fuscum*, indicating bog conditions.

Table 1. Description of all sites including region, coordinates, peatland type, active layer depth at the time of sampling (cm), number of samples for Hg analysis, surface vegetation and reference publication.

Site	Region	Coordinates	Peatland Type	Active Layer Depth (cm)	# Samples For Hg Analysis	Surface Vegetation	Reference
Ennadai Lake	West-central Canada	60°83'33''N; -101°55'00''E	Polygonal Peat Plateau	41 (2002)	44	Ericaceae, lichen, dwarfed *Betula*	Sannel and Kuhry (2008)
Selwyn Lake	West-central Canada	59°88'33''N; -104°20'00''E	Peat Plateau	47 (1993)	77	*Picea mariana*, *Rhododendron tomentosum*, lichen	Sannel and Kuhry (2008)
McClintock	Hudson-Bay Lowlands	57°83'33''N; -94°20'00''E	Peat Plateau	30 (1992)	34	Sparse dwarfed *Picea mariana*, *Rhododendron tomentosum*, lichen	Kuhry (2008)
Herchmer Palsa	Hudson-Bay Lowlands	57°83'33''N; -94°18'30''E	Palsa	40 (1992)	34	*Picea mariana*, dwarfed Ericaceae, *Rubus chamaemorus*, lichen	Kuhry (2008)
Alvi	Dávvavuopmi, northern Sweden	68°27'51" N; 20°54'05"E	Peat Plateau	60 (2012)	19	Dwarf shrubs (*Empetrum nigrum ssp. hermaphroditu m*, *B. nana, Vaccinium ligunosum ssp. uligunosum , V. vitis-idaea, V. microcarpum, An dromeda polifolia), Rubus chamaemorus,* lichens and mosses (*Polytrichum juniperinum*, *Dicranum elongatum*)	Sannel *et al.* (2018)
Dávva	Dávvavuopmi, northern Sweden	68°27'51" N; 20°54'26"E	Peat Plateau	72 (2012)	10		Sannel *et al.* (2018)
Karlebotn	Finnmark, northern Norway	70°7'14" N; 28°28'30" E	Peat Plateau	65 (2016)	12	Dwarf shrubs (*E. nigrum ssp. hermaphroditu m*, *Rhododendron tomentosum*, *Vaccinium uliginosum*, *V. vitis-idaea*, *B. nana and Andromeda polifolia*), mosses (e.g. *Polytrichum commune*), lichen (*Cladonia spp.*) and *Rubus chamaemorus.*	Kjellmann *et al.* (2018)
Lakselv	Finnmark, northern Norway	70°7'15" N; 24°59'47" E	Peat Plateau	60 (2016)	10		Kjellmann *et al.* (2018)
Šuoššjávri	Finnmark, northern Norway	69°23'2" N; 24°15'27" E	Peat Plateau	60 (2016)	24		Kjellmann *et al.* (2018)

Laboratory Analysis

In total we analysed 264 samples from 9 peat cores for total mercury (Hg). All samples have been stored frozen at the facilities at Stockholm University until subsampled for this study. The samples were freeze-dried (Heto dry winner 6-55) and homogenised (mortar and spatula) prior to analysis. To determine Hg concentration (reported per dry weight of soil), a Milestone DMA-80 (Direct Mercury Analyzer) with direct thermal decomposition, amalgamation and atomic absorption spectrophotometry (AAS) with a wavelength of 254 nm (US EPA, 2007) was used. An internal reference material (210 ± 10 μg kg^{-1}) was analysed and the concentrations ranged from 202.2 to 218.8 μg kg^{-1}, with a mean of 210.4 μg kg^{-1}, a standard deviation (SD) of 4.6 μg kg^{-1} and relative standard deviation (RSD) of 2.2% (n = 24). Replicate samples (n = 9) ranged from 0.3 to 5.6 μg kg^{-1} (SD) and had an RSD between 2.2 to 12.96 %. Macrofossil data was retrieved from previous publications (Table 1). For this study, we focus on dark roots derived from *Picea* and/or *Larix* and Ericaceae (%Dark roots), which are considered dry peat surface indicators in peat plateaus and palsas (Sannel & Kuhry, 2009).

Data treatment

Earlier sampling strategies based on macrofossil analysis of the cores identified different peat horizons within them. The Ennadai and Selwyn Lake profiles, for example, were highly stratified, while the Scandinavian cores had a more homogeneous profile. The data generated for the concentrations of Hg and data used from previous studies thus varies in resolution among the cores and with core depth. To calculate average concentrations of Hg and other relevant parameters for the entire peat profile as well as individual dated subsections of the cores, depth weighted averages were computed and unsampled depth intervals were interpolated based on adjacent data points. Samples from the underlying mineral layer (defined as soil with < 17 % SOC; n = 23), which was reached in some but not all peat cores, were excluded from the calculated averages and further data analysis. The normality of the data was tested using the Shapiro-Wilk normality test. If needed (e.g. for THg and C/N), the data was log-transformed prior to statistical testing in order to reach normal distribution. In some cases where normality test failed but the p value was close to 0.05, the data was assumed to be normally distributed after visual inspection of the density plot. If data was not normally distributed, non-parametric testing followed using the Wilcoxon test, a non-parametric multiple comparison. Both this test and linear regression analysis were used to examine statistical differences among groups (including site, region, permafrost formation type) and correlations among variables. All statistical tests were carried out using JMP Pro (version 15.0.0) and significance was indicated by $p < 0.05$.

To identify transient peaks in the Hg depth profiles, we used the LOESS/LOWESS method (Locally Weighted Scatterplot Smoothing) from the loess function in R studio (version 4.4.2; R Core Team, 2022). Hereby, the baseline trend for Hg concentrations was estimated using weighted neighbours. Peaks were then isolated by comparing the smoothed baseline curve to the original data and identifying spikes above the smoothed trend (threshold: 1, span: 0.2) for each core (Figure S1). For %Dark roots this could not be carried out since the data points were too sparse.

To calculate consistent age-depth models for all cores, we recalibrated all radiocarbon dates with OxCal 4.4 (Bronk Ramsey, 2021) and the IntCal20 dataset (Reimer *et al.*, 2020). Calibrated median ages, using 2 standard deviations (2σ), were used for further calculations. The cumulated mass of Hg (µg Hg m^{-2}) and C (g C m^{-2}) of each core section was calculated as the respective sum of each section, where individual samples have been calculated by multiplying the dry bulk density (DBD, g cm^{-3}) with the respective concentration of Hg (µg kg^{-1}) and C (g C g^{-1} $soil^{-1}$) and the length (cm) of the section. Net Hg- and C-ARs (µg Hg m^{-2} yr^{-1} and g C m^{-2} yr^{-1}, respectively) were then calculated for each dated core section (i.e. sections between two dated layers) by dividing the cumulative mass of Hg and C, respectively, within this section with the time period (yr) under which the peat section had accumulated (age of lower dated layer – age of upper dated layer). Peat ARs (mm yr^{-1}) were calculated in a similar fashion by dividing height of the section with the time period. The presented rates refer to the net accumulation over time, reflecting the sum of multiple processes. As the radiocarbon dates were recalibrated using an updated age-model for this study, our reported peat and C-ARs are close, but not identical, to those previously reported from some of these cores (Table 1, respective references). The rates calculated for the uppermost section of each of the peat cores, representing most recent ARs, covered periods ranging from 116 cal. yr BP to 2643 cal. yr BP. No direct comparison of these most recent Hg, C and peat AR was done, as they cover time periods that are not comparable. As discussed later on, these most recent ARs are also influenced by modern atmospheric Hg levels and were thus excluded from further analysis (Figure S2). Henceforth, all Hg-AR and C-AR refer to the rates calculated for sections without the uppermost layer unless otherwise stated.

To examine the influence of different peat accumulation stages, Hg concentration and C/N were estimated for successional peat stages in the peatland development, with peat succession stages based on plant macrofossil assemblages from original publications (Table 1). Hereby, the distinction between peat stages is based on differences in hydrological conditions and vegetation composition. Dry bogs have a lower water table and are characterised by wood, roots, *Ericaceous* shrubs and *Polytrichum* and *Dicranum* mosses, while moist bogs have slightly higher water table with occasional saturation and are often dominated by *Sphagnum fuscum* moss. Wet fens have a consistently high or near surface water table and are characterised by wet Sphagna, brown mosses and graminoids. Identified palsa stages (dry bogs) were treated separately from other dry bogs due to their unique properties, including e.g. dry surface, more exposure for wind erosion and slower peat accumulation rates (Zoltai, 1972; Sollid & Sørbel, 1998).

RESULTS AND DISCUSSION

Concentrations and accumulation rates of Hg

Across all peat samples, we observe Hg concentrations ranging from 4 to 220 µg kg^{-1}. When comparing cores from different geographical regions (cores from the sporadic permafrost region in northern Scandinavia vs. cores from the discontinuous and continuous permafrost region in Canada), no significant difference in Hg averages were observed (Table S2). Summary statistics of all investigated parameters can be found in the supporting information (Table S1). In line with previous studies of permafrost peatlands in Scandinavia (e.g. Klaminder *et al.*, 2008; Tarbier *et al.*, 2021), as well as peatlands elsewhere (e.g. Roos-Barraclough *et al.*, 2002), we observe higher concentrations of Hg in the uppermost peat layer (Table S2). For the top 20 cm of the peat, the average

Hg concentrations were 1.4 – 10 times higher compared to subsurface peat layers (Table S2), which overlaps with the estimated range (3 – 5 times) of increased atmospheric concentrations for the industrialization era compared to the pre-industrial background (Biester *et al.*, 2007; Bindler *et al.*, 2001).

Using available ^{14}C-dates of the cores, accumulation rates for Hg as well as C and peat were calculated (Table 2 and S3). For the uppermost peat layer, estimated Hg-AR ranged from 0.16 to 18.6 µg Hg m^{-2} yr^{-1} across all sites (Table S3). These rates are in the lower range of earlier estimates of modern Hg-ARs in peat reported from the northern hemisphere (8 – 184 µg Hg m^{-2} yr^{-1}, Biester *et al.*, 2007, and references therein; 6.6 ± 1.6 to 14 ± 4.8 µg Hg m^{-2} yr^{-1}, Li *et al.*, 2023; 5.2 ± 1.2 µg Hg m^{-2} yr^{-1}, Dastoor *et al.*, 2022). It should be noted that our estimated rates for the most recent time period evaluated are based on averages for the uppermost peat layer which represents a large timespan (116 to 2643 cal. yr. BP), while the largest increase in atmospheric Hg levels likely occurred from the 1760's to 1880's (Amos *et al.*, 2015). The rates estimated for the uppermost sections are thus not comparable to each other nor necessarily representative of modern Hg-ARs. The estimated Hg-ARs in the uppermost peat layer may, as discussed further below, also have been influenced by slower peat accumulation in the uppermost peat that consisted of rootlet layers. Due to these constraints, C and Hg-AR were not evaluated further for the uppermost section and all analysis done further below is based on the subsurface peat sections.

In the subsurface peat sections of the profiles, Hg-AR ranged from 0.30 to 16.3 µg Hg m^{-2} yr^{-1} (Table 2). We do not see a statistical difference for Hg-AR when comparing Canadian and Scandinavian peat cores ($p = 0.5$, One-way ANOVA, Student t-test). This suggests either that centennial and millennial atmospheric Hg levels are recorded similarly in both regions or that a large within-region variability is obscuring any regional differences. As previously concluded by Biester *et al*., (2007), caution should be taken when using peat to reconstruct past atmospheric Hg levels due to the many environmental processes involved. This complexity is also evident in our peat cores, e.g. from the coupling of Hg concentrations to trends in macrofossil patterns.

Table 2. Information of permafrost zone, permafrost formation, peat accumulation rate (peat AR, mm yr^{-1}), carbon accumulation rate (C-AR, g C m^{-2} yr^{-1}), Hg accumulation rate (µg Hg m^{-2} yr^{-1}) and C-normalized Hg-AR (µg Hg g C^{-1} m^{-2} yr^{-1}) for each site with the uppermost peat layer excluded (Figure S1). Means and standard deviation shown for both regions: northern Scandinavia and Canada.

Region	Site	Permafrost zone	Permafrost formation	peat AR (mm yr^{-1})	C-AR (g C m^{-2} yr^{-1})	Hg-AR (µg Hg m^{-2} yr^{-1})	C-normalized Hg-AR (µg Hg g C^{-1} m^{-2} yr^{-1})
Northern Scandinavia	**Alvi**	Sporadic	Epigenetic	0.21	14	0.82	0.06
	Dávva [1)]	Sporadic	Epigenetic	0.10	9.0	0.73	0.08
	Karlebotn	Sporadic	Epigenetic	0.26	16	1.0	0.06
	Lakselv	Sporadic	Epigenetic	0.28	12	1.5	0.13
	Šuoššjávri [1)]	Sporadic	Epigenetic	0.24	16	1.3	0.08
Canada	**Ennadai Lake**	Continuous	Syngenetic	0.70	22	0.74	0.03
	Herschmer Palsa	Discontinuous	Epigenetic	0.25	18	2.0	0.11
	McClintock	Continuous	Epigenetic	0.28	16	1.5	0.09
	Selwyn Lake	Discontinuous	Syngenetic	0.38	17	1.0	0.06
	Av SCAN			0.22 ± 0.06	13 ± 2.5	1.1 ± 0.30	0.08 ± 0.02
	Av CAN			0.40 ± 0.18	18 ± 2.2	1.3 ± 0.48	0.07 ± 0.03

[1)] Two points were considered outliers due to anomalous C-AR (Davva. 78.75 cm: 209.2 g C m^{-2} yr^{-1}; Šuoššjávri 226.3 cm: 77.7 g C m^{-2} yr^{-1}).

Hg accumulation of past peat succession stages

Combining detailed peat accumulation histories from plant macrofossil analysis with Hg data allows us to explore net accumulation of Hg under different peat stages in investigated cores. Foliar uptake of atmospheric Hg^0, followed by the incorporation of plant material into litter, has been identified as the main pathway by which mercury enters peat deposits (Obrist *et al*., 2017; Sun & Branfireun, 2023). As the concentration of Hg in peat parent material (litter from surface vegetation) may vary with vegetation type (Enrico *et al.*, 2016; Li *et al.*, 2025) and peat ARs (Biester *et al.*, 2003), past accumulation conditions could help to explain variations of Hg within and among the peat cores.

For the Scandinavian cores, the plant macrofossil analysis indicate that most of the peat has accumulated under a fen stage (Sannel *et al.*, 2018). Throughout the subsurface sections, consistently low %Dark roots suggest that the peat developed under relatively constant conditions. In these layers, we also see uniform concentrations of Hg, never exceeding a value of ~ 50 μg kg^{-1} (Figure 2-10). In contrast, the upper peat layer shows a distinct shift in macrofossil assemblages, suggesting that a dry peat plateau or palsa only developed more recently, along with higher concentrations of Hg. As the concentrations of Hg in the uppermost layers may have been influenced by modern Hg levels, the evaluation below focuses on an analysis of the subsurface sections (Figure S2). We do, however, note that the higher Hg surface concentrations in these (and the Canadian) cores, in addition to elevated modern atmospheric concentrations of Hg, could be the result of slower peat ARs in the upper rootlet layers, allowing more time for Hg to accumulate per volume of litter as discussed further below (Biester *et al.*, 2003; Rydberg *et al.*, 2010a).

In contrast to northern Scandinavia, the plant macrofossil analysis in the Canadian cores suggested a more dynamic peat formation history. Also, the concentration of Hg in the subsurface peat varied to a larger extent in these cores (Figure 2-5, Table S2). This was especially prominent in the twosyngenetic peat cores (Ennadai and Selwyn Lake), where several peaks in Hg concentration were observed in the subsurface peat sections (Figure 2-3). The peat in these cores, which mainly developed under moister conditions (characterised by the dominant *Sphagnum fuscum* peat) were often interspersed with layers representing drier conditions (rootlet peat layers) (Sannel & Kuhry, 2008). When comparing the position of the peaks of Hg with the results of the macrofossil analysis, most identified Hg peaks occurred in layers with elevated values of %Dark roots (e.g.: Selwyn Lake, at 42 – 43 cm, Figure 3). Also, the subsurface layers of the two Canadian cores with epigenetic permafrost aggradation history (Herchmer Palsa, McClintock) have developed under different peat succession stages (e.g. dry bog, wet fen). Two peaks in Hg concentration were also identified in the subsurface peat of the McClintock (Figure 4). Sudden increases in %Dark roots, as seen in the Ennadai and Selwyn Lake cores, were however not present.

The %Dark roots indicate drier surface conditions and slower peat AR at the time of peat formation. Earlier studies have demonstrated that growth rate may influence the concentration of Hg in surface vegetation. For example Sun & Branfireun (2023) observed seasonal differences in Hg levels, with lower foliar Hg concentrations during the grown season, in a boreal peatland and suggested that these differences may be explained by growth dilution. Differences in growth rate has also been suggested as a contributing factor explaining higher concentrations of Hg observed in non-vascular plants, in comparison to vascular plants in Arctic tundra systems (Olson *et al.*, 2019). It may appear counterintuitive that drier conditions, and the presence of vascular plants e.g. leaves (higher %Dark roots), would result in higher Hg levels as these plants typically contain lower tissue concentrations of Hg (Olson *et al.*, 2019). The peat in these layers, however, is in most sections mostly made up of non-vascular plants like *Sphagnum* spp. Non-vascular plants have a large surface area and can live for decades (Riis *et al.*, 2014; Shahid *et al.*, 2017), both factors that contribute considerably to increased accumulation of Hg. We therefore suggest that the higher concentration of Hg in the rootlet layers reflect slower growth rates of these non-vascular plants under drier conditions, leading to enhanced Hg accumulation. Other possible explanations linked to changes in atmospheric Hg deposition for the detected Hg peaks, including volcanic eruptions (as observed, for example, in glacial ice cores; Schuster *et al.*, 2002), are considered unlikely, as we would then expect more consistent patterns across cores, at least on a regional scale. Although peaks in Hg did not always coincide with higher %Dark roots, these results demonstrate the importance of understanding past peat accumulation conditions when interpreting the vertical Hg profile in peat cores.

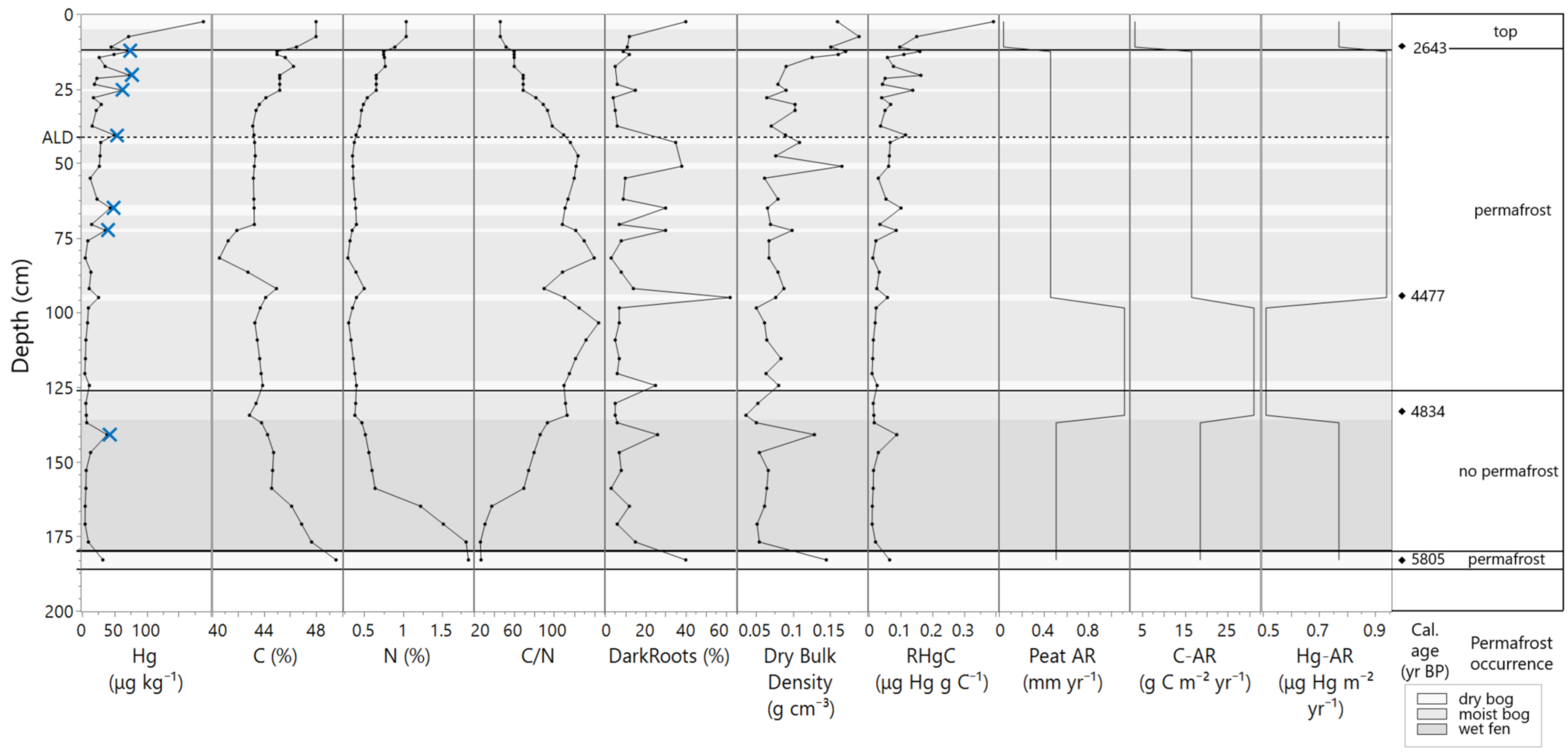

Figure 2. Ennadai Lake peat profile showing the vertical distribution of mercury concentration (Hg, µg kg^{-1}), carbon (C, %), nitrogen (N, %), C/N ratio, dark roots (%), dry bulk density (DBD, g cm^{-3}) and Hg normalised to C (RHgC, µg Hg g C^{-1}). Peat accumulation rate (Peat AR, mm yr^{-1}), carbon accumulation rate (C-AR, g C m^{-2} yr^{-1}) and mercury accumulation rate (Hg-AR, µg Hg m^{-2} yr^{-1}) presented have been estimated for dated depth intervals. Calibrated age (yr BP) and permafrost occurrence (solid lines) are shown on the right side. Peat stages are indicated with shaded colors. Dotted line at 41 cm represents the active layer depth at the time of sampling (2002). If peaks in Hg concentrations were detected, these are marked with a blue cross. Profiles of C, N, C/N, DarkRoots and DBD adjusted after Sannel & Kuhry (2008).

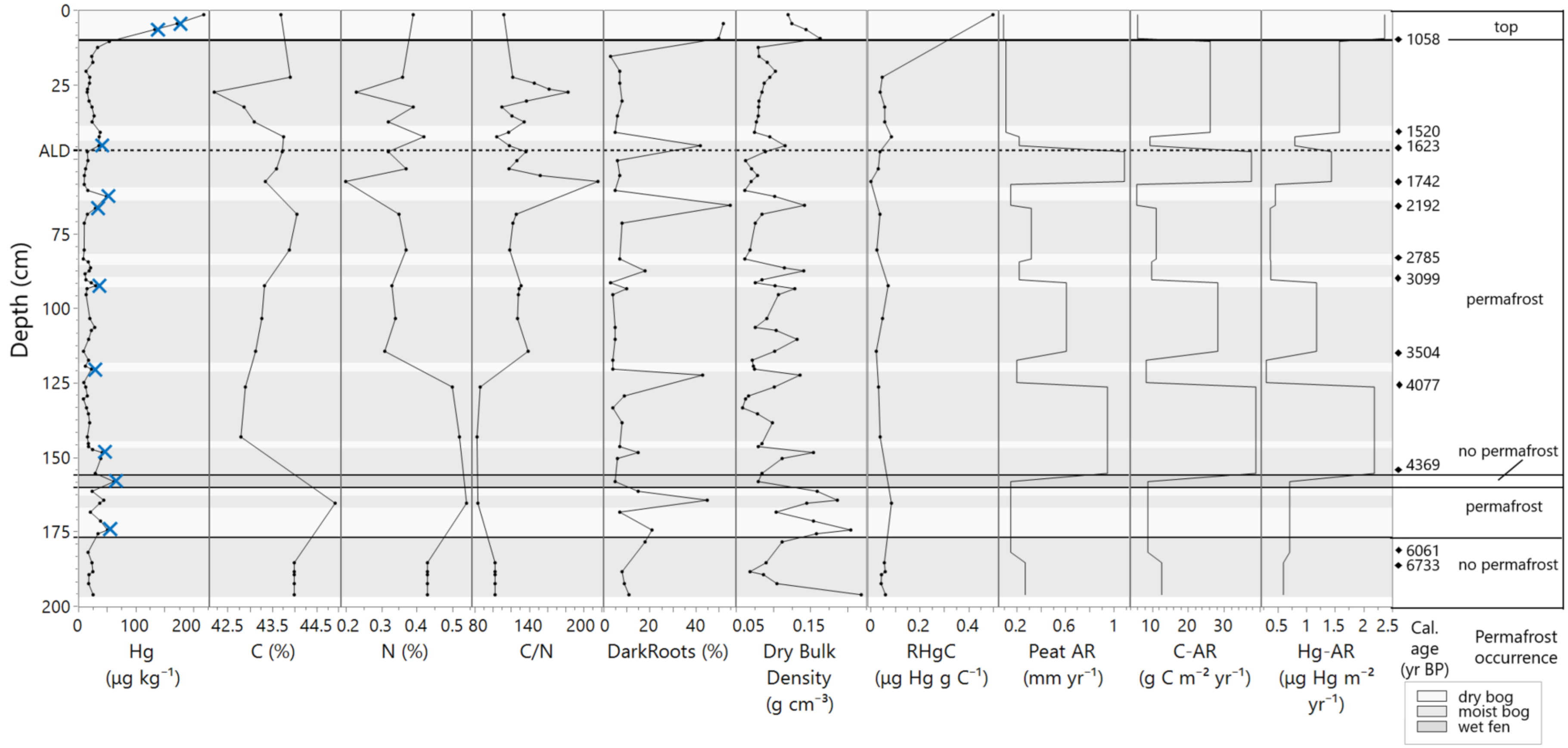

Figure 3. Selwyn Lake peat profile showing vertical distribution of mercury concentration (Hg, µg kg^{-1}), carbon (C, %), nitrogen (N, %), C/N ratio, dark roots (%), dry bulk density (DBD, g cm^{-3}) and Hg normalised to C (RHgC, µg Hg g C^{-1}). Peat accumulation rate (peat AR, mm yr^{-1}), carbon accumulation rate (g C m^{-2} yr^{-1}) and mercury accumulation rate (µg Hg m^{-2} yr^{-1}) have been estimated for dated depth intervals. Calibrated age (yr BP) as well as permafrost occurrence (solid lines) are on the right side. Peat stages are indicated with shaded colors. Dotted line at 47 cm represents the active layer depth at the time of sampling (1993). If peaks in Hg concentrations were detected, these are marked with a blue cross. Profiles of C, N, C/N, DarkRoots and DBD adjusted after Sannel & Kuhry (2008).

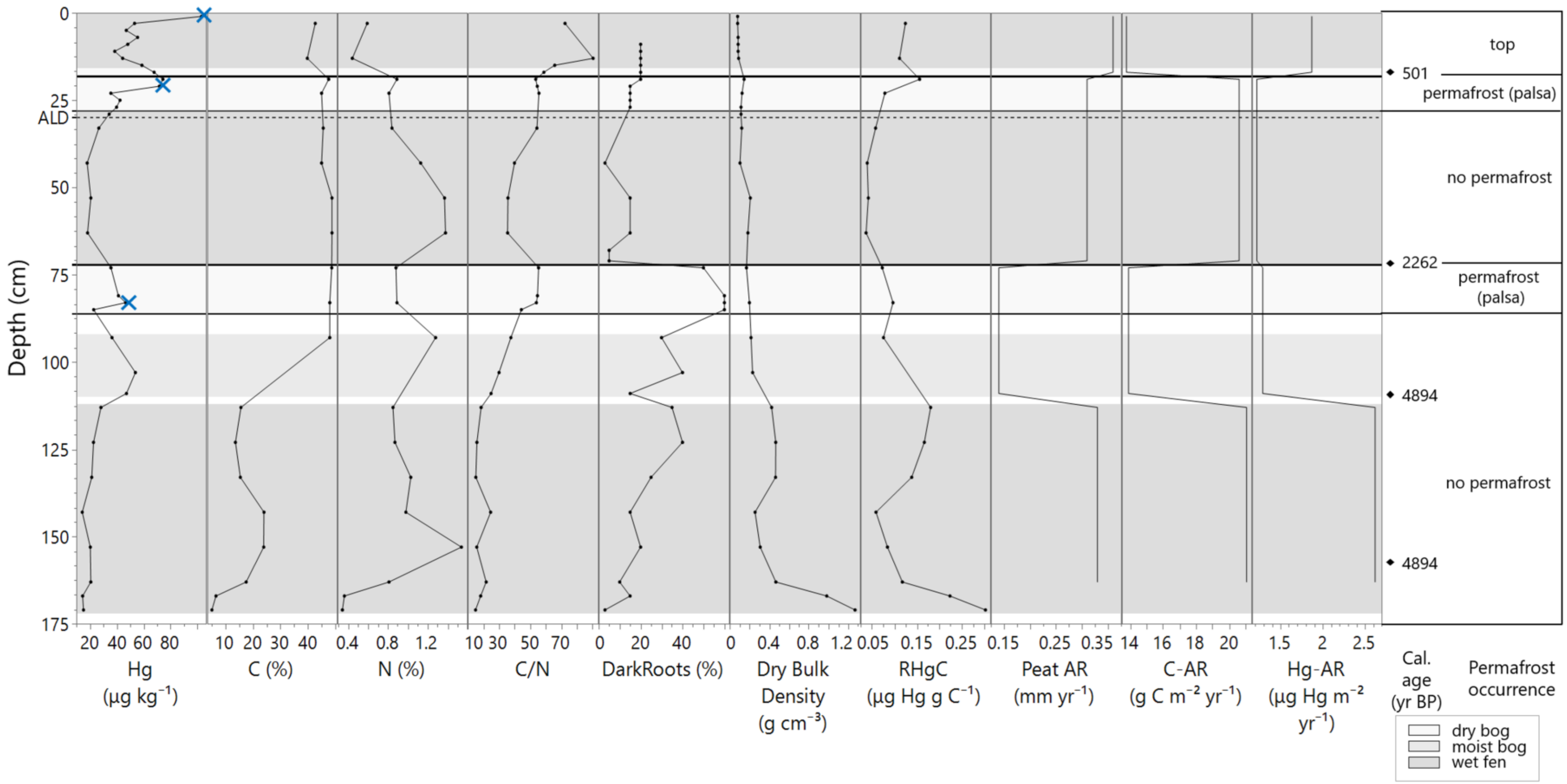

Figure 4. McClintock peat profile showing vertical distribution of mercury concentration (Hg, µg kg^{-1}), carbon (C, %), nitrogen (N, %), C/N ratio, dark roots (%), dry bulk density (DBD, g cm^{-3}) and Hg normalised to C (RHgC, µg Hg g C^{-1}). Peat accumulation rate (peat AR, mm yr^{-1}), carbon accumulation rate (C-AR, g C m^{-2} yr^{-1}) and mercury accumulation rate (Hg-AR, µg Hg m^{-2} yr^{-1}) have been estimated for dated depth intervals. Calibrated age (yr BP) as well as permafrost occurrence (solid lines) are on the right side. Peat stages are indicated with shaded colors. Dotted line at 30 cm represents the active layer depth at the time of sampling (1992). If peaks in Hg concentrations were detected, these are marked with a blue cross. Profiles of C, N, C/N, DarkRoots and DBD adjusted after Kuhry (2008).

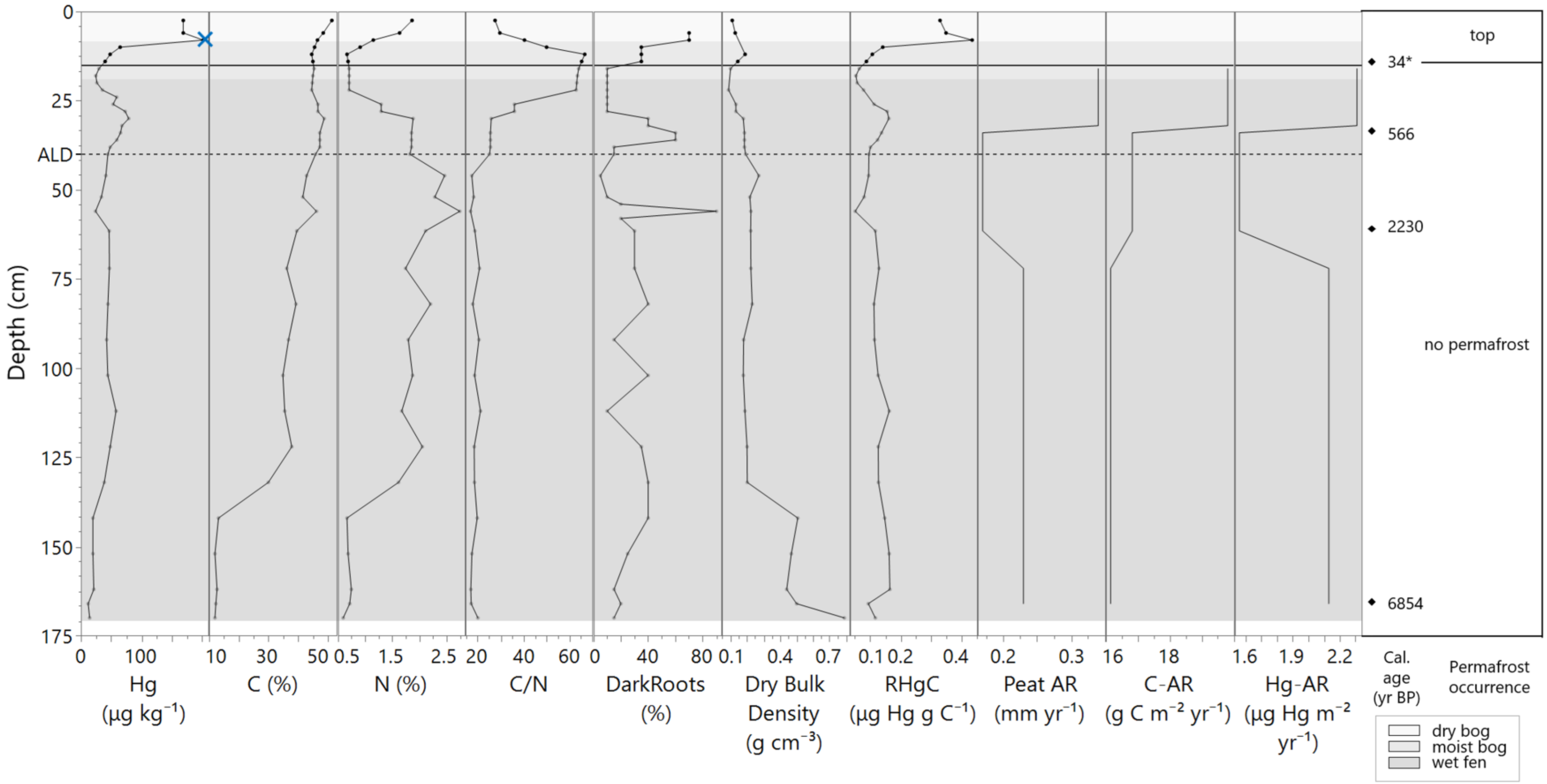

Figure 5. Herchmer Palsa peat profile showing vertical distribution of mercury concentration (Hg, µg kg^{-1}), carbon (C, %), nitrogen (N, %), C/N ratio, dark roots (%), dry bulk density (DBD, g cm^{-3}) and Hg normalised to C (RHgC, µg Hg g C^{-1}). Peat accumulation rate (peat AR, mm yr^{-1}), carbon accumulation rate (C-AR, g C m^{-2} yr^{-1}) and mercury accumulation rate (Hg-AR, µg Hg m^{-2} yr^{-1}) have been estimated for dated depth intervals. Calibrated age (yr BP) as well as permafrost occurrence (solid lines) are on the right side. Peat stages are indicated with shaded colors. Dotted line at 40 cm represents the active layer depth at the time of sampling (1992). If peaks in Hg concentrations were detected, these are marked with a blue cross. Profiles of C, N, C/N, DarkRoots and DBD adjusted after Kuhry (2008). * stands for modern age results and excluded outliers above for ARs (Table S3).

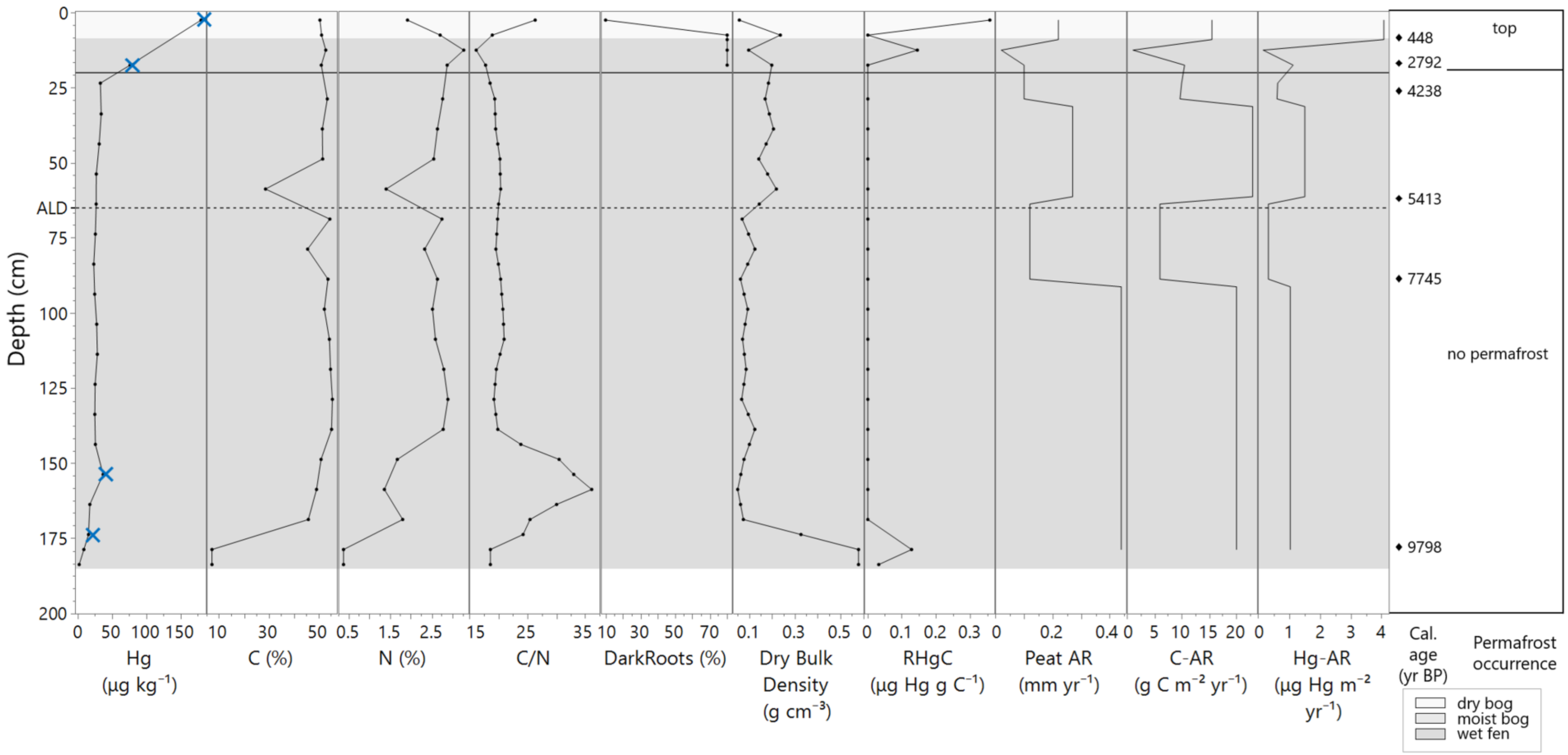

Figure 6. Alvi peat profile showing vertical distribution of mercury concentration (Hg, µg kg^{-1}), carbon (C, %), nitrogen (N, %), C/N ratio, dark roots (%), dry bulk density (DBD, g cm^{-3}) and Hg normalised to C (RHgC, µg Hg g C^{-1}). Peat accumulation rate (peat AR, mm yr^{-1}), carbon accumulation rate (C-AR, g C m^{-2} yr^{-1}) and mercury accumulation rate (Hg-AR, µg Hg m^{-2} yr^{-1}), have been estimated for dated depth intervals. Calibrated age (yr BP) as well as permafrost occurrence (solid lines) are on the right side. Peat stages are indicated with shaded colors. Dotted line at 65 cm represents the active layer depth at the time of sampling (2012). If peaks in Hg concentrations were detected, these are marked with a blue cross. Profiles of C, N, C/N, DarkRoots and DBD adjusted after Sannel *et al.*, (2018).

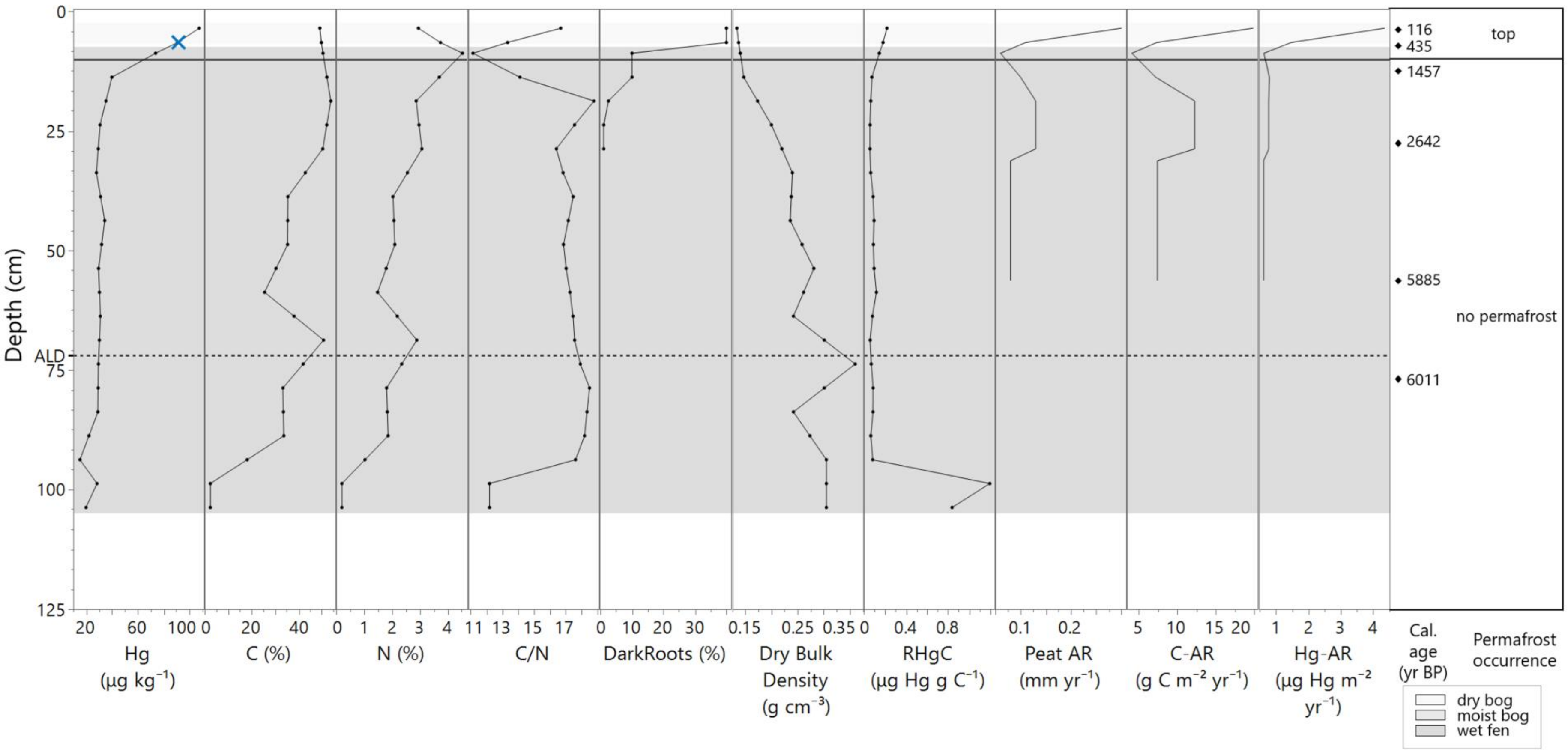

Figure 7. Dávva peat profile showing vertical distribution of mercury concentration (Hg, µg kg^{-1}), carbon (C, %), nitrogen (N, %), C/N ratio, dark roots (%), dry bulk density (DBD, g cm^{-3}) and Hg normalised to C (RHgC, µg Hg g C^{-1}). Peat accumulation rate (peat AR, mm yr^{-1}), carbon accumulation rate (C-AR, g C m^{-2} yr^{-1}) and mercury accumulation rate (Hg-AR, µg Hg m^{-2} yr^{-1}) have been estimated for dated depth intervals. Calibrated age (yr BP) as well as permafrost occurrence (solid lines) are on the right side. Peat stages are indicated with shaded colors. Dotted line at 72 cm represents the active layer depth at the time of sampling (2012). If peaks in Hg concentrations were detected, these are marked with a blue cross. Profiles of C, N, C/N, DarkRoots and DBD adjusted after Sannel *et al*., (2018).

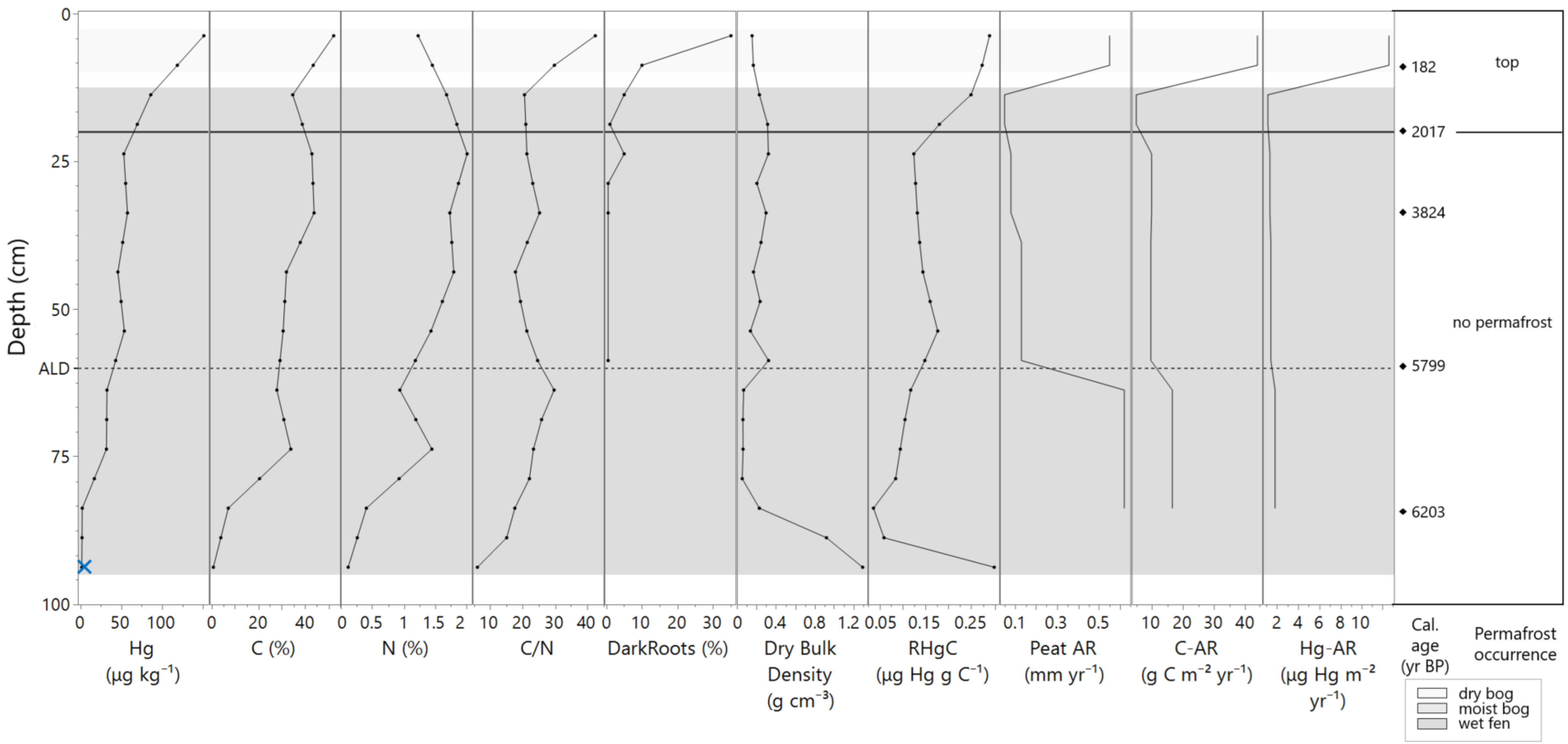

Figure 8. Lakselv peat profile showing vertical distribution of mercury concentration (Hg, µg kg^{-1}), carbon (C, %), nitrogen (N, %), C/N ratio, dark roots (%), dry bulk density (DBD, g cm^{-3}) and Hg normalized to C (RHgC, µg Hg g C^{-1}). Peat accumulation rate (peat AR, mm yr^{-1}), carbon accumulation rate (C-AR, g C m^{-2} yr^{-1}) and mercury accumulation rate (Hg-AR, µg Hg m^{-2} yr^{-1}) have been estimated for dated depth intervals. Calibrated age (yr BP) as well as permafrost occurrence (solid lines) are on the right side. Peat stages are indicated with shaded colors. Dotted line at 60 cm represents the active layer depth at the time of sampling (2016). If peaks in Hg concentrations were detected, these are marked with a blue cross. Profiles of C, N, C/N, DarkRoots and DBD adjusted after Kjellmann *et al.* (2018).

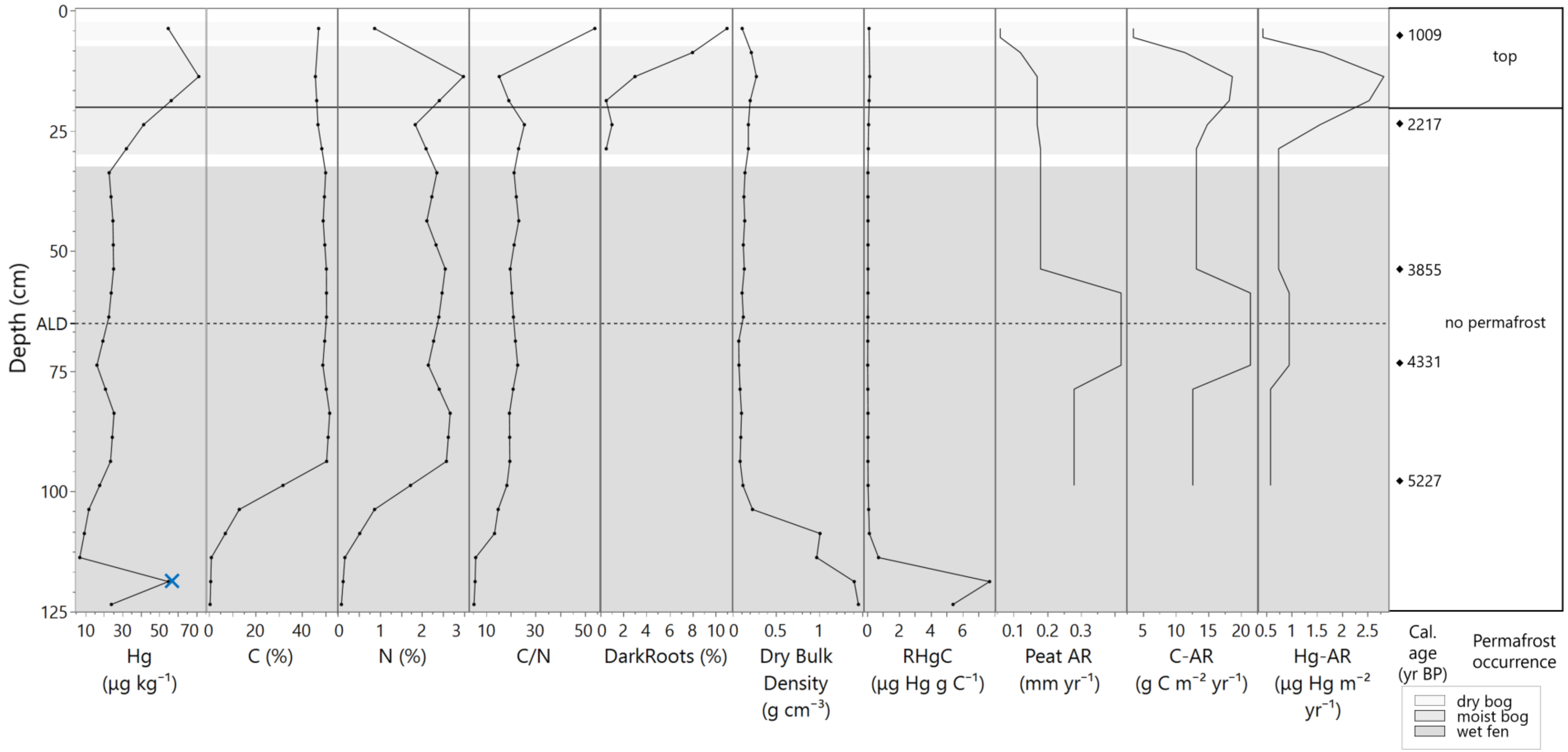

Figure 9. Karlebotn peat profile showing vertical distribution of mercury concentration (Hg, µg kg^{-1}), carbon (C, %), nitrogen (N, %), C/N ratio, dark roots (%), dry bulk density (DBD, g cm^{-3}) and Hg normalised to C (RHgC, µg Hg g C^{-1}). Peat accumulation rate (peat AR, mm yr^{-1}), carbon accumulation rate (C-AR, g C m^{-2} yr^{-1}) and mercury accumulation rate (Hg-AR, µg Hg m^{-2} yr^{-1}) have been estimated for dated depth intervals. Calibrated age (yr BP) as well as permafrost occurrence (solid lines) are on the right side. Peat stages are indicated with shaded colors. Dotted line at 65 cm represents the active layer depth at the time of sampling (2016). If peaks in Hg concentrations were detected, these are marked with a blue cross. Profiles of C, N, C/N, DarkRoots and DBD adjusted after Kjellmann *et al.* (2018).

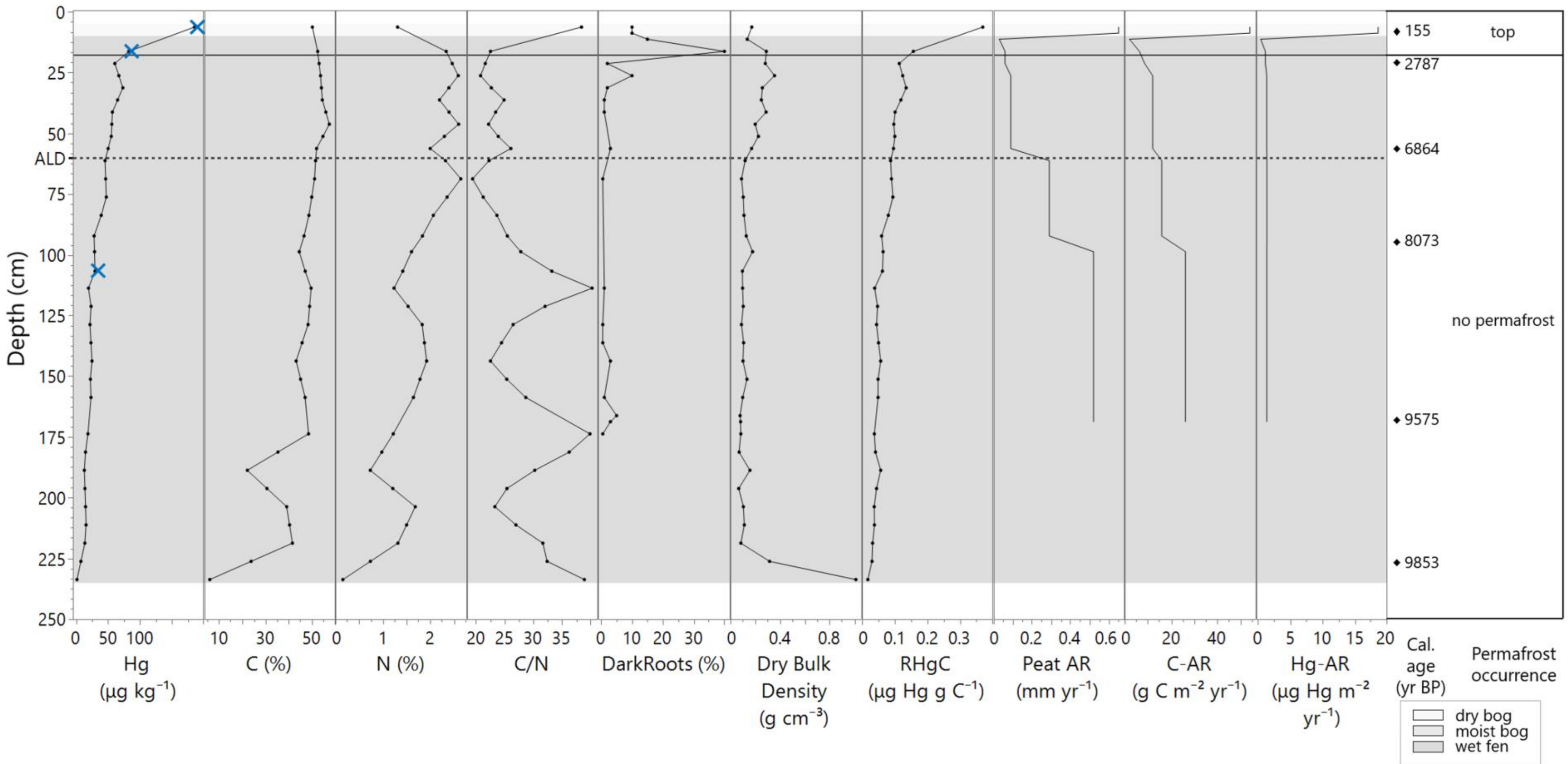

Figure 10. Šuoššjávri peat profile showing vertical distribution of mercury concentration (Hg, µg kg^{-1}), carbon (C, %), nitrogen (N, %), C/N ratio, dark roots (%), dry bulk density (DBD, g cm^{-3}) and Hg normalised to C (µg Hg g C^{-1}). Peat accumulation rate (peat AR, mm yr^{-1}), carbon accumulation rate (C-AR, g C m^{-2} yr^{-1}) and mercury accumulation rate (Hg-AR, µg Hg m^{-2} yr^{-1}) have been estimated for dated depth intervals. Calibrated age (yr BP) as well as permafrost occurrence (solid lines) are on the right side. Peat stages are indicated with shaded colors. Dotted line at 60 cm represents the active layer depth at the time of sampling (2016). If peaks in Hg concentrations were detected, these are marked with a blue cross. Profiles of C, N, C/N, DarkRoots and DBD adjusted after Kjellmann *et al.* (2018).

When comparing Hg concentrations across peat sections that accumulated during different peat stages (associated with different degree of wetness and peat ARs), we observe differences such as higher concentrations of Hg in dry bog on palsas (Figure 11). Palsas are more exposed to environmental stressors such as wind and thus drier conditions due to their elevated nature. Consequently, palsa peat is typically associated with slower peat ARs (Zoltai, 1972) compared to dry bogs on other landforms. It is possible that this has contributed to the elevated Hg concentrations observed in the dry bog stages with palsas. Because the available ^{14}C radiocarbon dated sections that include palsa dry bog also in part include other peat stages, we were unable to test this hypothesis on our current dataset. We cannot in our data distinguish the influence of growth dilution and differences in peat decomposition rates. The C/N ratio was also lower in dry bog with palsas in comparison to e.g. non-palsa dry bog (Figure 11). Lower degree of peat degradation could thus also have contributed to the lower Hg concentration in this peat stage, as discussed further below. It should also be noted that no clear differences in Hg concentrations were observed between non-palsa dry bogs and stages with wetter surface conditions, stages where differences in ARs also would be expected. Furthermore, the elevated Hg concentrations in palsa dry bogs were relatively modest, with median values of 27 and 41 μg kg^{-1} in non-palsa and palsa dry bogs, respectively. We therefore conclude that while peat succession stages may help explain local subsurface Hg peaks in high-resolution profiles, they appear to be less predictive of net Hg-ARs over longer time periods.

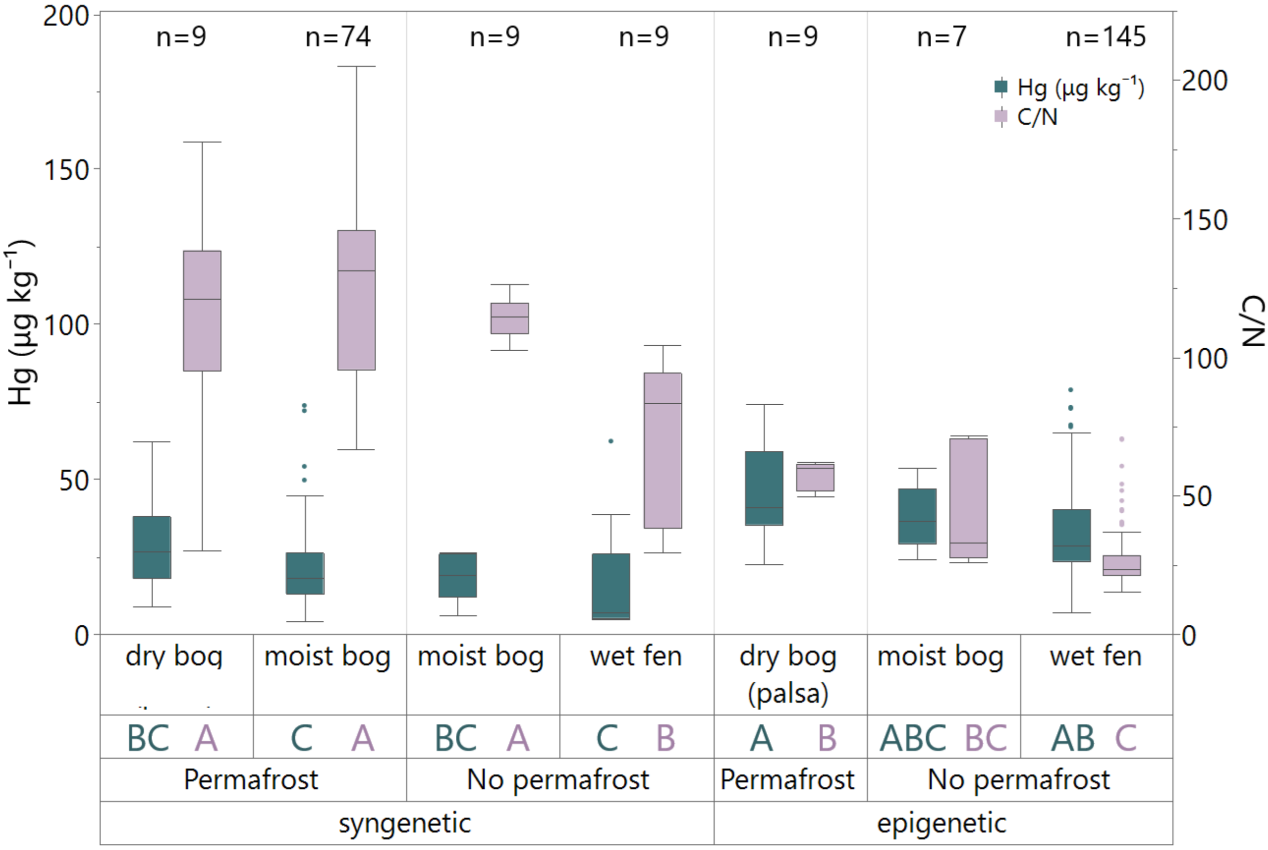

Figure 11. Hg concentration (μg kg^{-1}) and C/N ratios in subsurface peat succession stages. Boxes represent the 25th and 75th percentiles, horizontal lines indicate the median, whiskers show the interquartile range, and points represent outliers. Green and purple letters indicate significant differences ($p < 0.05$) in Hg concentration and C/N respectively, between each peat stage and represent non-parametric multiple comparison test results (Wilcoxon test).

Role of C accumulation rates, peat decomposition and permafrost history

When comparing C- and Hg-AR, we can see that Hg-ARs in this study follow those of C (Figure 12, Table S4). The Hg-C relationship persists in ARs through depth sections and permafrost formation types (syngenetic: $p = 0.0007$; epigenetic: $p = 0.0035$). The observed relationship between Hg- and C-ARs is well aligned with earlier observations (e.g. Håkanson *et al.*, 1990; Grigal, 2003; Lim *et al.*, 2020) and fits the current consensus that Hg accumulation in peat is driven by litter deposition (Jiskra *et al.*, 2015; Obrist *et al.*, 2017), where up to 90 % of Hg is taken up by atmospheric Hg^0 deposition (Enrico *et al.*, 2016; Li *et al.*, 2023) rather than abiotic deposition pathways. As suggested by the slope of the regression lines (Figure 12), C-AR increases twice as fast as Hg-AR, a phenomenon that could be due to growth dilution of Hg. Decreasing Hg concentrations in the vegetation from a sedge dominated peatland during the growing season have also been previously demonstrated (Sun & Branfireun, 2023). In agreement with the higher Hg concentrations found in some of the peat layers formed under conditions associated with lower peat ARs, the faster increase in C-AR (and positive intercept of the regression lines), suggest more Hg to accumulate per litter mass when the C-AR is low.

Recorded Hg-AR and C-AR will not only depend on past litter production, but also the degree of peat degradation (e.g. Biester *et al.*, 2003; Rydberg *et al.*, 2010b). Peat in permafrost regions is of particular interest with this respect, as the permafrost may protect peat from further degradation. Our data includes both syn- and epigenetic permafrost systems. In line with earlier work (e.g. Treat *et al.*, 2016), we observe significantly higher C/N in the syngenetic peat cores (Figure 13), supporting less decomposed peat due to the simultaneous formation of peat and permafrost. At the same time, the offset between Hg-AR vs. C-AR regression lines for epi- and syngenetic permafrost shows approximately twice as much Hg accumulation for the same C accumulation in epigenetic permafrost peat deposits (Figure 12). This is likely due to peat decomposition under non-permafrost conditions where C is removed but Hg, at least partly, can be expected to retained resulting in a higher Hg to C ratio. We also recorded lower concentrations of Hg and lower Hg to C ratio in the two syngenetic cores from Canada, in comparison to the two epi-genetic cores from the same region (Figure 13). These findings suggest that while C accumulation is a strong control over Hg accumulation in the litter, peat decomposition may increase Hg concentration post-deposition. The range of Hg concentrations and Hg to C ratio recorded from the Scandinavian cores (all epigenetic permafrost), however, overlaps with the values from the Canadian syngenetic cores, suggesting that spatial heterogeneity may be as important as permafrost history. It is important to note that peat degradation still may have contributed to release of Hg from our peat deposits, as we do not know the quantity of C that has been lost post-deposition. Peat decomposition that follows permafrost collapse under certain conditions can also result in lower Hg concentrations, for example when comparing dry and intact peat plateaus with collapsed and inundated peat as a result of permafrost thaw (Klaminder *et al.*, 2008; Fahnestock *et al.*, 2019).

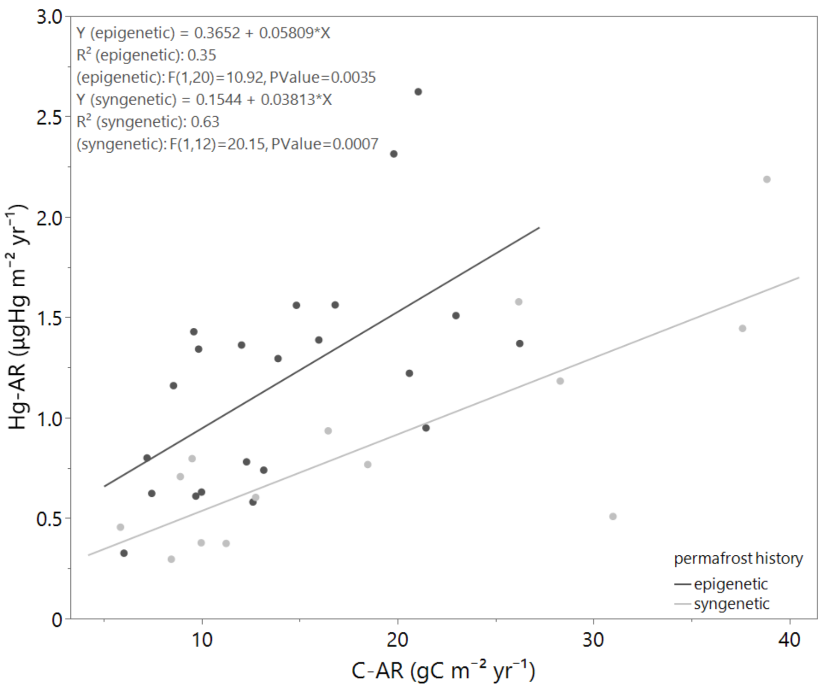

Figure 12. Linear regression between net Hg and C accumulation rates (Hg-AR, µg Hg m^{-2} yr^{-1} and C-AR, g C m^{-2} yr^{-1}, respectively) in subsurface peat across the dated depth intervals for both permafrost formation types (epigenetic and syngenetic). Comparison of the two linear regressions yield a significant difference of intercept ($p<0.0001$). Note that the x-axis does not reach zero. Excluded are two data points where C-AR were considered outliers (Davva: 209.2 g C m^{-2} yr^{-1} at 78.75 cm; Šuoššjávri 77.7 g C m^{-2} yr^{-1} at 226.3 cm).

Enrichment of Hg to C ratio due to peat decomposition has also been previously observed (Rydberg *et al.*, 2010b; Biester *et al.*, 2003; Giesler *et al.*, 2017). There are several processes in which the Hg also may be remobilised during peat decomposition (Beckers & Rinklebe, 2017). Microbial processes, could for example convert the Hg stored in the peat into gaseous Hg^0 (Wiatrowski *et al.*, 2006). In addition, degradation of particulate OM could liberate Hg from the peat matrix and make it available for relocation through movement of pore water. Due to Hg's strong affinity to the particulate phase (also including Hg in its gaseous form, Hg^0), its mobility in organic rich systems is, however, low, contributing to the retention of Hg (e.g. Montoya *et al.*, 2019). Past ARs could also have been affected by physical peat erosion processes (by e.g. wind erosion), this is, however, less likely to alter the ratio of Hg to C in the peat deposit. Some of the earlier work linking Hg to C ratios to peat decomposition has relied on C/N ratios to track the peat degradation state (Rydberg *et al.*, 2010b; Biester *et al.*, 2003). Although differences between the epi- and syngenetic cores were observed, neither Hg nor the Hg to C ratio correlated with the C/N in the epigenetic peat deposits. For most of these cores, there was also no significant relationship between RHgC or Hg concentration and C/N, and among the few cores with significant correlations, no consistent trend was observed (Figure S3). The C/N in peat primarily depends on plant composition (Kuhry & Vitt, 1996), which can mask effects of peat decomposition. The effect of peat decomposition on Hg levels may thus be challenging to follow using C/N unless there are large differences in the degree of degradation, as observed here for the epi- and syngenetic cores.

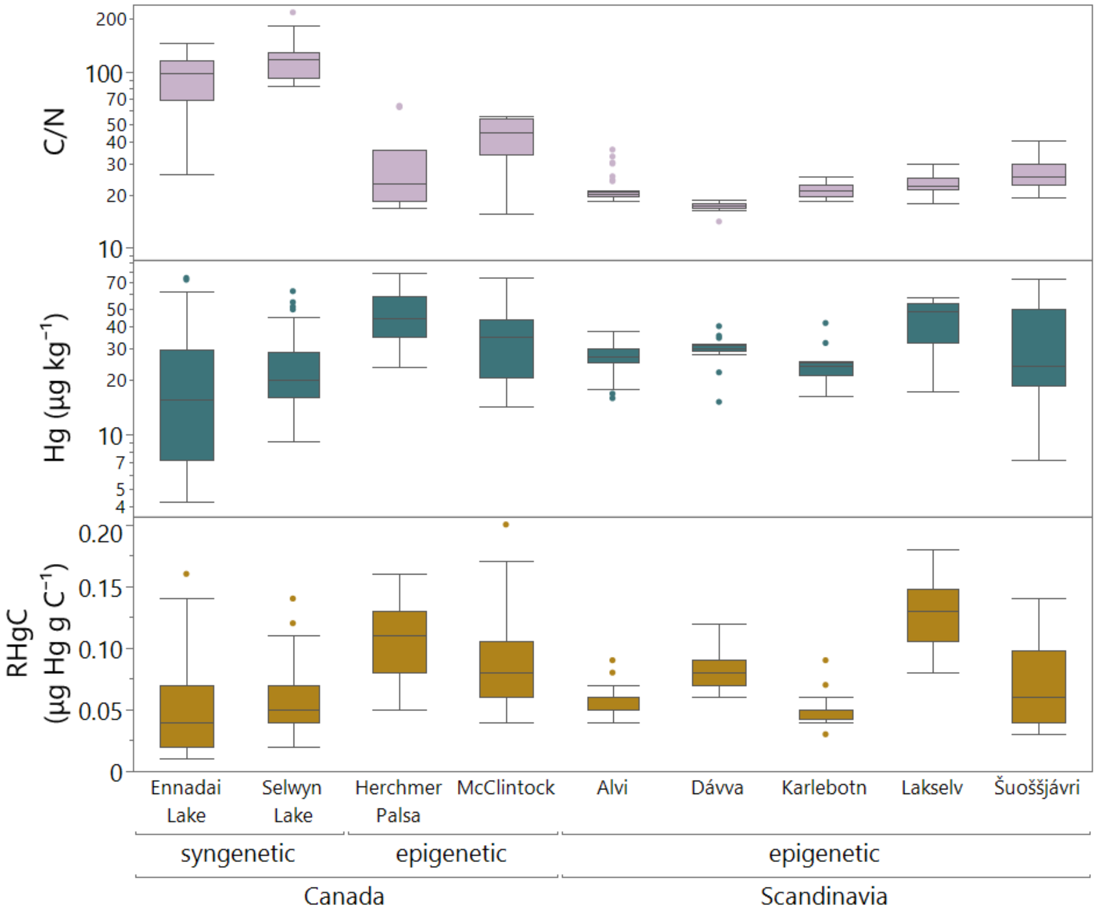

Figure 13. C/N, Hg concentration ($\mu g\ kg^{-1}$) and RHgC (μg Hg g C^{-1}) for subsurface peat of individual sites (Figure S1), grouped by permafrost formation history (syngenetic, epigenetic) and region (Canada, Scandinavia). Boxes represent the 25th and 75th percentiles, horizontal lines indicate the median, whiskers show the interquartile range, and points represent outliers. Note that the upper two panels have a log scale.

In line with data from e.g. Lim *et al.*, (2020), we did not observe an apparent shift in Hg concentrations at the permafrost table (transition between the permafrost and the active layer at the time of sampling; Figure 2-10). When the active layer thickens as permafrost thaws, fresh organic material is exposed for microbial processes and Hg may be reduced and mobilized. Previous studies demonstrated elevated Hg porewater concentration at the thaw front (Sirota *et al.*, 2020). Although the active layer thickness can fluctuate annually and has thickened over recent decades with an average rate of 0.11 cm yr^{-1} in northern permafrost regions (CALM (Circumpolar Active layer Monitoring); Liu *et al.*, 2024), the absence of a distinct change in Hg levels at the current permafrost table in our cores suggests that Hg concentrations remain stable, regardless of whether the soil thaws seasonally in recent years. We also note that permafrost at Herchmer Palsa, in contrast to the other sites, occurred relatively recently (dated to AD 1958 ± 3 yr, 30 years before sampling) and have remained permafrost free for the majority of the peat accumulation period. Despite this, no clear trends in Hg concentrations or C/N ratios were observed at Herchmer Palsa compared to other sites with epigenetic permafrost (Figure 13). This suggests that neither the current depth of the permafrost table nor the age of permafrost formation plays a major role in controlling Hg concentrations in these peat deposits.

Environmental Implications

Northern peatlands have acted as important sinks for both C and Hg for millennia. With the accelerated warming of the Arctic, Hg locked in permafrost peatlands is at risk of being remobilised (Lim *et al.*, 2020; Schaefer *et al.*, 2020), which may worsen Hg exposure among Arctic wildlife and northern communities. However, the future transformation of Arctic landscapes will be characterised by high spatial and temporal heterogeneity (Siewert *et al.*, 2021). By exploring past Hg accumulation history in well-characterised peat cores, our study helps shed light on how these complex alterations of the Arctic landscape may perturb the Hg cycle.

Anthropogenic Hg emissions have significantly influenced atmospheric Hg concentrations with notable effects on Hg deposition and its accumulation in peatlands. Pre-industrial Hg-ARs in peat were up to 15 times lower compared to those during the industrial period up until ca. 1990 (Steinnes & Sjøbakk, 2005). Following emission reduction measures, Hg emissions decreased across Europe by ca. 60% (1990-2011) (UNECE, 2012). If emissions are further mitigated, this may also contribute to lower global atmospheric Hg levels, which would also impact the net accumulation of Hg in northern peatlands. A study from northern Sweden has, indeed, already demonstrated a shift in a peatland that, due to lower atmospheric concentrations of Hg, has turned from a sink to a source of Hg to the atmosphere (Osterwalder *et al.*, 2017). Here, reemission of Hg^0 was far greater than stream Hg export and peak evasion during summer corresponded to highest radiation. This trend suggests that future changes in Hg atmospheric concentrations influence the role of peatland ecosystems as sink or source for the Hg cycle. To predict the future role of the Arctic terrain in the global cycling of Hg, what regulates the net accumulation of Hg in permafrost peat deposits needs to be better constrained. Here, we present data showing how peat accumulation conditions, carbon accumulation rates and permafrost history influence Hg concentration in permafrost peatlands. These insights can help refine estimates of current Hg stocks in thawing permafrost regions and improve our understanding of how future Arctic change may affect the net accumulation of Hg in permafrost peatlands.

ACKNOWLEDGEMENTS

We are grateful to Dr Karin Helmens and Ms Maija Kahanpaa for field support in collecting the peat profiles in Canada. We would also like to thank Ms Pia Axelsson and Dr Sofia Kjellman for support during field sampling in Norway, and Mr Alexander Kessler, Mr Jesper Sannel and Dr Vilmantas Prėskienis in Sweden. We thank Anna Hägglund for support during analysis of mercury and with coaching the master students.

This research was funded by the European Union's Horizon 2020 research and innovation programme under the Marie Sklodowska-Curie (grant agreement no. 860497, to SJ), the European Union Horizon 2020 research and innovation project Nunataryuk (grant agreement no. 773421, to GH), and the Swedish Research Council for Environment, Agricultural Sciences and Spatial Planning (FORMAS; no. 2020-01868 and 2023-01561, to SJ). We further acknowledge the following agencies and organisations for funding the original fieldwork: Bolin Centre for Climate Research, Canadian Circumpolar Institute (University of Alberta, Edmonton, Canada), Knut and Alice Wallenberg Foundation, Research Council of Norway (no. 244903/E10 & no. 255331), FORMAS (no. 214–2014-562), Swedish Society for Anthropology and Geography (SSAG) and Ymer-80 Foundation.

AUTHOR CONTRIBUTIONS

SJ initiated and designed this project. Data and samples were provided by BS, PK and GH, while laboratory analysis was done by BT and AB as part of their respective master thesis. CH assembled all data and led all further data analysis. CH led manuscript writing with support from SJ. CH, BS, PK, GH and SJ provided comments.

REFERENCES

AMAP Assessment 2021: Mercury in the Arctic | AMAP. (n.d.). Retrieved May 31, 2023, from https://www.amap.no/documents/doc/amap-assessment-2021-mercury-in-the-arctic/3581

Amos, H. M., Sonke, J. E., Obrist, D., Robins, N., Hagan, N., Horowitz, H. M., Mason, R. P., Witt, M., Hedgecock, I. M., Corbitt, E. S., & Sunderland, E. M. (2015). Observational and Modeling Constraints on Global Anthropogenic Enrichment of Mercury. *Environmental Science & Technology*, *49*(7), 4036–4047. https://doi.org/10.1021/es5058665

Beckers, F., & Rinklebe, J. (2017). Cycling of mercury in the environment: Sources, fate, and human health implications: A review. *Critical Reviews in Environmental Science and Technology*, *47*(9), 693–794. https://doi.org/10.1080/10643389.2017.1326277

Biester, H., Bindler, R., Martinez-Cortizas, A., & Engstrom, D. R. (2007). Modeling the Past Atmospheric Deposition of Mercury Using Natural Archives. *Environmental Science & Technology*, *41*(14), 4851–4860. https://doi.org/10.1021/es0704232

Biester, H., Martinez-Cortizas, A., Birkenstock, S., & Kilian, R. (2003). Effect of Peat Decomposition and Mass Loss on Historic Mercury Records in Peat Bogs from Patagonia. *Environmental Science & Technology*, *37*(1), 32–39. https://doi.org/10.1021/es025657u

Bindler, R., Olofsson, C., Renberg, I., & Frech, W. (2001). Temporal Trends in Mercury Accumulation in Lake Sediments in Sweden. *Water, Air, and Soil Pollution: Focus 1*, 343–355.

Bronk Ramsey, C. (2021). *OxCal version 4.4 (Computer program)*. University of Oxford Radiocarbon Accelerator Unit. https://c14.arch.ox.ac.uk/oxcal/OxCal.html

CALM (Circumpolar Active layer Monitoring). (n.d.). *CALM Site*. Circumpolar Active Layer Monitoring. Retrieved July 31, 2025, from https://www2.gwu.edu/~calm/

Charman, D. J., Beilman, D. W., Blaauw, M., Booth, R. K., Brewer, S., Chambers, F. M., Christen, J. A., Gallego-Sala, A., Harrison, S. P., Hughes, P. D. M., Jackson, S. T., Korhola, A., Mauquoy, D., Mitchell, F. J. G., Prentice, I. C., Van Der Linden, M., De Vleeschouwer, F., Yu, Z. C., Alm, J., … Zhao, Y. (2013). Climate-related changes in peatland carbon accumulation during the last millennium. *Biogeosciences*, *10*(2), 929–944. https://doi.org/10.5194/bg-10-929-2013

Dastoor, A., Angot, H., Bieser, J., Christensen, J. H., Douglas, T. A., Heimbürger-Boavida, L.-E., Jiskra, M., Mason, R. P., McLagan, D. S., Obrist, D., Outridge, P. M., Petrova, M. V., Ryjkov, A., St. Pierre, K. A., Schartup, A. T., Soerensen, A. L., Toyota, K., Travnikov, O., Wilson, S. J., & Zdanowicz, C. (2022). Arctic mercury cycling. *Nature Reviews Earth & Environment*, *3*(4), 270–286. https://doi.org/10.1038/s43017-022-00269-w

Enrico, M., Le Roux, G., Marusczak, N., Heimbürger, L.-E., Claustres, A., Fu, X., Sun, R., & Sonke, J. E. (2016). Atmospheric Mercury Transfer to Peat Bogs Dominated by Gaseous Elemental Mercury Dry Deposition. *Environmental Science & Technology*, *50*(5), 2405–2412. https://doi.org/10.1021/acs.est.5b06058

Fahnestock, M. F., Bryce, J. G., McCalley, C. K., Montesdeoca, M., Bai, S., Li, Y., Driscoll, C. T., Crill, P. M., Rich, V. I., & Varner, R. K. (2019). Mercury reallocation in thawing subarctic peatlands. *Geochemical Perspectives Letters (Online)*, *11*. https://doi.org/10.7185/geochemlet.1922

Giesler, R., Clemmensen, K. E., Wardle, D. A., Klaminder, J., & Bindler, R. (2017). Boreal Forests Sequester Large Amounts of Mercury over Millennial Time Scales in the Absence of Wildfire. *Environmental Science & Technology*, *51*(5), 2621–2627. https://doi.org/10.1021/acs.est.6b06369

Gorham, E. (1991). Northern Peatlands: Role in the Carbon Cycle and Probable Responses to Climatic Warming. *Ecological Applications*, *1*(2), 182–195. https://doi.org/10.2307/1941811

Grigal, D. F. (2003). Mercury Sequestration in Forests and Peatlands: A Review. *Journal of Environmental Quality*, *32*(2), 393–405. https://doi.org/10.2134/jeq2003.3930

Håkanson, L., Nilsson, Å., & Andersson, T. (1990). Mercury in the Swedish mor layer? linkages to mercury deposition and sources of emission. *Water, Air, and Soil Pollution*, *50*(3–4), 311–329. https://doi.org/10.1007/BF00280632

Hichens-Bergström, M., & Sannel, A. B. K. (2023). Permafrost development in northern Fennoscandian peatlands since the mid-Holocene.

Arctic, Antarctic, and Alpine Research, *55*(1), 2250035. https://doi.org/10.1080/15230430.2023.2250035

Hugelius, G., Loisel, J., Chadburn, S., Jackson, R. B., Jones, M., MacDonald, G., Marushchak, M., Olefeldt, D., Packalen, M., Siewert, M. B., Treat, C., Turetsky, M., Voigt, C., & Yu, Z. (2020). Large stocks of peatland carbon and nitrogen are vulnerable to permafrost thaw. *Proceedings of the National Academy of Sciences*, *117*(34), 20438–20446. https://doi.org/10.1073/pnas.1916387117

Jiskra, M., Sonke, J. E., Obrist, D., Bieser, J., Ebinghaus, R., Lund Myhre, C., Pfaffhuber, K. A., Wängberg, I., Kyllönen, K., Worthy, D., Martin, L. G., Labuschagne, C., Mkololo, T., Ramonet, M., Magand, O., & Dommergue, A. (2018). A vegetation control on seasonal variations in global atmospheric mercury concentrations. *Nature Geoscience*, *11*(4), 244-250. https://doi.org/10.1038/s41561-018-0078-8

Jiskra, M., Wiederhold, J. G., Skyllberg, U., Kronberg, R.-M., Hajdas, I., & Kretzschmar, R. (2015). Mercury Deposition and Re-emission Pathways in Boreal Forest Soils Investigated with Hg Isotope Signatures. *Environmental Science & Technology*, *49*(12), 7188–7196. https://doi.org/10.1021/acs.est.5b00742

Kjellman, S. E., Axelsson, P. E., Etzelmüller, B., Westermann, S., & Sannel, A. B. K. (2018). Holocene development of subarctic permafrost peatlands in Finnmark, northern Norway. *The Holocene*, *28*(12), 1855–1869. https://doi.org/10.1177/0959683618798126

Klaminder, J., Yoo, K., Rydberg, J., & Giesler, R. (2008). An explorative study of mercury export from a thawing palsa mire. *Journal of Geophysical Research: Biogeosciences*, *113*(G4), G04034. https://doi.org/10.1029/2008JG000776

Kuhry, P. (1998). Late Holocene permafrost dynamics in two Subarctic peatlands of the Hudson Bay Lowlands (Manitoba, Canada). *Eurasian soil science, 31*(5), 529–534.

Kuhry, P. (2008). Palsa and peat plateau development in the Hudson Bay Lowlands, Canada: Timing, pathways and causes. *Boreas*, *37*(2), 316–327. https://doi.org/10.1111/j.1502-3885.2007.00022.x

Kuhry, P., & Vitt, D. H. (1996). Fossil Carbon/Nitrogen Ratios as a Measure of Peat Decomposition. *Ecology*, *77*(1), 271–275. https://doi.org/10.2307/2265676

Li, C., Enrico, M., Bishop, K., Roberts, S. J., Hodgson, D. A., Lamentowicz, M., Mauquoy, D., Mestrot, A., & Grosjean, M. (2025). Perspectives on using peat records to reconstruct past atmospheric Hg levels. *Journal of Hazardous Materials*, *482*, 136581. https://doi.org/10.1016/j.jhazmat.2024.136581

Li, C., Jiskra, M., Nilsson, M. B., Osterwalder, S., Zhu, W., Mauquoy, D., Skyllberg, U., Enrico, M., Peng, H., Song, Y., Björn, E., & Bishop, K. (2023). Mercury deposition and redox transformation processes in peatland constrained by mercury stable isotopes. *Nature Communications*, *14*(1), 7389. https://doi.org/10.1038/s41467-023-43164-8

Lim, A. G., Jiskra, M., Sonke, J. E., Loiko, S. V., Kosykh, N., & Pokrovsky, O. S. (2020). A revised pan-Arctic permafrost soil Hg pool based on Western Siberian peat Hg and carbon observations. *Biogeosciences*, *17*(12), 3083–3097. https://doi.org/10.5194/bg-17-3083-2020

Liu, Z., Kimball, J. S., Ballantyne, A., Watts, J. D., Natali, S. M., Rogers, B. M., Yi, Y., Klene, A. E., Moghaddam, M., Du, J., & Zona, D. (2024). Widespread deepening of the active layer in northern permafrost regions from 2003 to 2020. *Environmental Research Letters*, *19*(1), 014020. https://doi.org/10.1088/1748-9326/ad0f73

Manies, K. L., Jones, M. C., Waldrop, M. P., Leewis, M., Fuller, C., Cornman, R. S., & Hoefke, K. (2021). Influence of Permafrost Type and Site History on Losses of Permafrost Carbon After Thaw. *Journal of Geophysical Research: Biogeosciences*, *126*(11), e2021JG006396. https://doi.org/10.1029/2021jg006396

Markkula, I., & Kuhry, P. (2020). Subfossil oribatid mite communities indicate Holocene permafrost dynamics in Canadian mires. *Boreas*, *49*(4), 730–738. https://doi.org/10.1111/bor.12444

Mathijssen, P. J. H., Gałka, M., Borken, W., & Knorr, K.-H. (2019). Plant communities control long term carbon accumulation and biogeochemical gradients in a Patagonian bog. *Science of The Total Environment*, *684*, 670–681. https://doi.org/10.1016/j.scitotenv.2019.05.310

Montoya, A. J., Lena, J. C., & Windmöller, C. C. (2019). Adsorption of gaseous elemental mercury on soils: Influence of chemical and/or mineralogical characteristics. *Ecotoxicology and Environmental Safety*, *170*, 98–106. https://doi.org/10.1016/j.ecoenv.2018.11.054

Obrist, D., Agnan, Y., Jiskra, M., Olson, C. L., Colegrove, D. P., Hueber, J., Moore, C. W., Sonke, J. E., & Helmig, D. (2017). Tundra uptake of atmospheric elemental mercury drives Arctic mercury pollution. *Nature*, *547*(7662), 201-204. https://doi.org/10.1038/nature22997

O'Donnell, J. A., Jorgenson, M. T., Harden, J. W., McGuire, A. D., Kanevskiy, M. Z., & Wickland,

K. P. (2012). The Effects of Permafrost Thaw on Soil Hydrologic, Thermal, and Carbon Dynamics in an Alaskan Peatland. *Ecosystems*, *15*(2), 213–229. https://doi.org/10.1007/s10021-011-9504-0

Oksanen, P. O., Kuhry, P., & Alekseeva, R. N. (2001). Holocene development of the Rogovaya River peat plateau, European Russian Arctic. *The Holocene*, *11*(1), 25–40. https://doi.org/10.1191/095968301675477157

Oksanen, P. O., Kuhry, P., & Alekseeva, R. N. (2003). Holocene Development and Permafrost History of the Usinsk Mire, Northeast European Russia. *Géographie Physique et Quaternaire*, *57*(2–3), 169–187. https://doi.org/10.7202/011312ar

Olson, C., Jiskra, M., Biester, H., Chow, J., & Obrist, D. (2018). Mercury in Active-Layer Tundra Soils of Alaska: Concentrations, Pools, Origins, and Spatial Distribution. *Global Biogeochemical Cycles*, *32*(7), 1058–1073. https://doi.org/10.1029/2017GB005840

Olson, C., Jiskra, M., Sonke, J. E., & Obrist, D. (2019). Mercury in tundra vegetation of Alaska: Spatial and temporal dynamics and stable isotope patterns. *Science of The Total Environment*, *660*, 1502–1512. https://doi.org/10.1016/j.scitotenv.2019.01.058

Osterwalder, S., Bishop, K., Alewell, C., Fritsche, J., Laudon, H., Åkerblom, S., & Nilsson, M. B. (2017). Mercury evasion from a boreal peatland shortens the timeline for recovery from legacy pollution. *Scientific Reports*, *7*, 16022. https://doi.org/10.1038/s41598-017-16141-7

Reimer, P. J., Austin, W. E. N., Bard, E., Bayliss, A., Blackwell, P. G., Bronk Ramsey, C., Butzin, M., Cheng, H., Edwards, R. L., Friedrich, M., Grootes, P. M., Guilderson, T. P., Hajdas, I., Heaton, T. J., Hogg, A. G., Hughen, K. A., Kromer, B., Manning, S. W., Muscheler, R., … Talamo, S. (2020). The IntCal20 Northern Hemisphere Radiocarbon Age Calibration Curve (0–55 cal kBP). *Radiocarbon*, *62*(4), 725–757. https://doi.org/10.1017/RDC.2020.41

Riis, T., Christoffersen, K. S., & Baattrup-Pedersen, A. (2014). Effects of warming on annual production and nutrient-use efficiency of aquatic mosses in a high Arctic lake. *Freshwater Biology*, *59*(8), 1622–1632. https://doi.org/10.1111/fwb.12368

Roos-Barraclough, F., Martinez-Cortizas, A., García-Rodeja, E., & Shotyk, W. (2002). A 14 500 year record of the accumulation of atmospheric mercury in peat: Volcanic signals, anthropogenic influences and a correlation to bromine accumulation. *Earth and Planetary Science Letters*, *202*(2), 435–451. https://doi.org/10.1016/S0012-821X(02)00805-1

Rydberg, J., Klaminder, J., Ròsen, & Bindler, R. (2010a). Climate driven release of carbon and mercury from permafrost mires increases mercury loading to sub-arctic lakes. *Science of The Total Environment*, *408*(20), 4778–4783. https://doi.org/10.1016/j.scitotenv.2010.06.056

Rydberg, J., Karlsson, J., Nyman, R., Wanhatalo, I., Näthe, K., & Bindler, R. (2010a). Importance of vegetation type for mercury sequestration in the northern Swedish mire, Rödmossamyran. *Geochimica et Cosmochimica Acta*, *74*(24), 7116–7126. https://doi.org/10.1016/j.gca.2010.09.026

Sannel, A. B. K., Hempel, L., Kessler, A., & Préskienis, V. (2018). Holocene development and permafrost history in sub-arctic peatlands in Tavvavuoma, northern Sweden. *Boreas*, *47*(2), 454–468. https://doi.org/10.1111/bor.12276

Sannel, A. B. K., & Kuhry, P. (2008). Long-term stability of permafrost in subarctic peat plateaus, west-central Canada. *The Holocene*, *18*(4), 589–601. https://doi.org/10.1177/0959683608089658

Sannel, A. B. K., & Kuhry, P. (2009). Holocene peat growth and decay dynamics in sub-arctic peat plateaus, west-central Canada. *Boreas*, *38*(1), 13–24. https://doi.org/10.1111/j.1502-3885.2008.00048.x

Schaefer, K., Elshorbany, Y., Jafarov, E., Schuster, P. F., Striegl, R. G., Wickland, K. P., & Sunderland, E. M. (2020). Potential impacts of mercury released from thawing permafrost. *Nature Communications*, *11*, 4650. https://doi.org/10.1038/s41467-020-18398-5

Schuster, P. F., Krabbenhoft, D. P., Naftz, D. L., Cecil, L. D., Olson, M. L., Dewild, J. F., Susong, D. D., Green, J. R., & Abbott, M. L. (2002). Atmospheric Mercury Deposition during the Last 270 Years: A Glacial Ice Core Record of Natural and Anthropogenic Sources. *Environmental Science & Technology*, *36*(11), 2303–2310. https://doi.org/10.1021/es0157503

Schuster, P. F., Schaefer, K. M., Aiken, G. R., Antweiler, R. C., Dewild, J. F., Gryziec, J. D., Gusmeroli, A., Hugelius, G., Jafarov, E., Krabbenhoft, D. P., Liu, L., Herman-Mercer, N., Mu, C., Roth, D. A., Schaefer, T., Striegl, R. G., Wickland, K. P., & Zhang, T. (2018). Permafrost Stores a Globally Significant Amount of Mercury. *Geophysical Research Letters*, *45*(3), 1463–1471. https://doi.org/10.1002/2017GL075571

Shahid, M., Dumat, C., Khalid, S., Schreck, E., Xiong, T., & Niazi, N. K. (2017). Foliar heavy metal uptake, toxicity and detoxification in plants:

A comparison of foliar and root metal uptake. *Journal of Hazardous Materials*, *325*, 36–58. https://doi.org/10.1016/j.jhazmat.2016.11.063

Siewert, M. B., Lantuit, H., Richter, A., & Hugelius, G. (2021). Permafrost Causes Unique Fine-Scale Spatial Variability Across Tundra Soils. *Global Biogeochemical Cycles*, *35*(3), e2020GB006659. https://doi.org/10.1029/2020GB006659

Sirota, J. I., Kolka, R. K., Sebestyen, S. D., & Nater, E. A. (2020). Mercury dynamics in the pore water of peat columns during experimental freezing and thawing. *Journal of Environmental Quality*, *49*(2), 404–416. https://doi.org/10.1002/jeq2.20046

Sollid, J. L., & Sørbel, L. (1998). Palsa Bogs as a Climate Indicator: Examples from Dovrefjell, Southern Norway. *Ambio, Research for Mountain Area Development: Europe*, *27*(4), 287–291. https://www.jstor.org/stable/4314737

Steinnes, E., & Sjøbakk, T. E. (2005). Order-of-magnitude increase of Hg in Norwegian peat profiles since the outset of industrial activity in Europe. *Environmental Pollution*, *137*(2), 365–370. https://doi.org/10.1016/j.envpol.2004.10.008

Sun, T., & Branfireun, B. A. (2023). Plant mercury accumulation and litter input to a Northern Sedge-dominated Peatland. *Biogeosciences*, *20*(14), 2971–2984. https://doi.org/10.5194/bg-20-2971-2023

Talbot, J., Moore, T. R., Wang, M., Ouellet Dallaire, C., & Riley, J. L. (2017). Distribution of lead and mercury in Ontario peatlands. *Environmental Pollution*, *231*, 890–898. https://doi.org/10.1016/j.envpol.2017.08.095

Tarbier, B., Hugelius, G., Sannel, A. B. K., Baptista-Salazar, C., & Jonsson, S. (2021). Permafrost Thaw Increases Methylmercury Formation in Subarctic Fennoscandia. *Environmental Science & Technology*, *55*(10), 6710–6717. https://doi.org/10.1021/acs.est.0c04108

Treat, C. C., Jones, M. C., Camill, P., Gallego-Sala, A., Garneau, M., Harden, J. W., Hugelius, G., Klein, E. S., Kokfelt, U., Kuhry, P., Loisel, J., Mathijssen, P. J. H., O'Donnell, J. A., Oksanen, P. O., Ronkainen, T. M., Sannel, A. B. K., Talbot, J., Tarnocai, C., & Väliranta, M. (2016). Effects of permafrost aggradation on peat properties as determined from a pan-Arctic synthesis of plant macrofossils. *Journal of Geophysical Research: Biogeosciences*, *121*(1), 78–94. https://doi.org/10.1002/2015JG003061

UNECE. (2012). *Hemispheric transport of air pollution 2010. Part B: Mercury, edited by: Pirrone, N. and Keating, T.* (Technical Report Air Pollution Studies No. 18). United Nation Publication. https://hero.epa.gov/hero/index.cfm/reference/details/reference_id/4678457

Vardy, S. R., Warner, B. G., Turunen, J., & Aravena, R. (2000). Carbon accumulation in permafrost peatlands in the Northwest Territories and Nunavut, Canada. *The Holocene*, *10*(2), 273–280. https://doi.org/10.1191/095968300671749538

Vitt, D. H., Halsey, L. A., Bauer, I. E., & Campbell, C. (2000). Spatial and temporal trends in carbon storage of peatlands of continental western Canada through the Holocene. *Canadian Journal of Earth Science*, *37(5)*, 683-693. https://doi.org/10.1139/e99-097

Wiatrowski, H. A., Ward, P. M., & Barkay, T. (2006). Novel Reduction of Mercury(II) by Mercury-Sensitive Dissimilatory Metal Reducing Bacteria. *Environmental Science & Technology*, *40*(21), 6690–6696. https://doi.org/10.1021/es061046g

Zoltai, S. C. (1972). Palsas and Peat Plateaus in Central Manitoba and Saskatchewan. *Canadian Journal of Forest Research*, *2*(3), 291–302. https://doi.org/10.1139/x72-046

Submitted 13 Dec 2024, revision 21 Aug 2025, revision 01 Apr, 2026
Editor: Colin McCarter

Author for correspondence: Dr. Sofi Jonsson, Department of Environmental Science and Analytical Chemistry, Stockholm University, Svante Arrheniusväg 8 C, 11418 Stockholm.
E-mail: sofi.jonsson@aces.su.se